

University of Windsor

Scholarship at UWindor

Electronic Theses and Dissertations

Theses, Dissertations, and Major Papers

1996

Critical behaviour in the gravitational collapse of the scalar field.

Andrew. DeBenedictis
University of Windsor

Follow this and additional works at: <https://scholar.uwindsor.ca/etd>

Recommended Citation

DeBenedictis, Andrew., "Critical behaviour in the gravitational collapse of the scalar field." (1996).
Electronic Theses and Dissertations. 1584.
<https://scholar.uwindsor.ca/etd/1584>

This online database contains the full-text of PhD dissertations and Masters' theses of University of Windsor students from 1954 forward. These documents are made available for personal study and research purposes only, in accordance with the Canadian Copyright Act and the Creative Commons license—CC BY-NC-ND (Attribution, Non-Commercial, No Derivative Works). Under this license, works must always be attributed to the copyright holder (original author), cannot be used for any commercial purposes, and may not be altered. Any other use would require the permission of the copyright holder. Students may inquire about withdrawing their dissertation and/or thesis from this database. For additional inquiries, please contact the repository administrator via email (scholarship@uwindsor.ca) or by telephone at 519-253-3000ext. 3208.

INFORMATION TO USERS

This manuscript has been reproduced from the microfilm master. UMI films the text directly from the original or copy submitted. Thus, some thesis and dissertation copies are in typewriter face, while others may be from any type of computer printer.

The quality of this reproduction is dependent upon the quality of the copy submitted. Broken or indistinct print, colored or poor quality illustrations and photographs, print bleedthrough, substandard margins, and improper alignment can adversely affect reproduction.

In the unlikely event that the author did not send UMI a complete manuscript and there are missing pages, these will be noted. Also, if unauthorized copyright material had to be removed, a note will indicate the deletion.

Oversize materials (e.g., maps, drawings, charts) are reproduced by sectioning the original, beginning at the upper left-hand corner and continuing from left to right in equal sections with small overlaps. Each original is also photographed in one exposure and is included in reduced form at the back of the book.

Photographs included in the original manuscript have been reproduced xerographically in this copy. Higher quality 6" x 9" black and white photographic prints are available for any photographs or illustrations appearing in this copy for an additional charge. Contact UMI directly to order.

UMI

A Bell & Howell Information Company
300 North Zeeb Road, Ann Arbor MI 48106-1346 USA
313/761-4700 800/521-0600



Critical Behaviour in the Gravitational Collapse of the Scalar Field

by

Andrew DeBenedictis

A Thesis

**Submitted to the Faculty of Graduate Studies and Research
through the Department of Physics
in Partial Fulfillment of the Requirements for
the Degree of Master of Science at the
University of Windsor**

**Windsor, Ontario, Canada
1996**



National Library
of Canada

Acquisitions and
Bibliographic Services

395 Wellington Street
Ottawa ON K1A 0N4
Canada

Bibliothèque nationale
du Canada

Acquisitions et
services bibliographiques

395, rue Wellington
Ottawa ON K1A 0N4
Canada

Your file Votre référence

Our file Notre référence

The author has granted a non-exclusive licence allowing the National Library of Canada to reproduce, loan, distribute or sell copies of this thesis in microform, paper or electronic formats.

The author retains ownership of the copyright in this thesis. Neither the thesis nor substantial extracts from it may be printed or otherwise reproduced without the author's permission.

L'auteur a accordé une licence non exclusive permettant à la Bibliothèque nationale du Canada de reproduire, prêter, distribuer ou vendre des copies de cette thèse sous la forme de microfiche/film, de reproduction sur papier ou sur format électronique.

L'auteur conserve la propriété du droit d'auteur qui protège cette thèse. Ni la thèse ni des extraits substantiels de celle-ci ne doivent être imprimés ou autrement reproduits sans son autorisation.

0-612-30898-7

A 66 072

© 1996 Andrew DeBenedictis
University of Windsor
Windsor, Ontario, Canada

Abstract

An in depth study of general relativistic gravitational collapse is done using the massless scalar field as the material model in a spherically symmetric space-time. Particular attention is paid to the critical regime which separates black hole formation and field dispersal. It is found that at this threshold certain field variables display discrete self-similarity with a period of $\Delta_r \approx e^{-3.45}$ and with each repetition on a spatial scale $\Delta_r \approx 31.4$ times smaller. These findings are in agreement with behaviour discovered by Choptuik. A study of black hole masses which form satisfies a power law with the critical exponent $\gamma \approx 0.364$. Also, it is found that near the origin there can exist regions of high curvature which will be visible to distant observers. Contrary to what was expected, bifurcation in the light cone structure near the origin between cases where infinitesimal mass black holes form and cases where conditions are slightly too weak to form a black hole is significant. The study does not use an adaptive mesh technique but instead utilizes null coordinates and an adaptive quadrature technique on a number of different initial data surface profiles therefore providing both independent verification of these phenomena as well as strong support for initial data independence.

For the Taxpayer.

There are many people whom I would like to acknowledge in regards to the preparation of this work. I would like to thank Dr. Edward Glass who helped make a difficult subject comprehensible and who always encouraged me to find out or work out the answers to difficulties. Discussions with Dr. Glass were invaluable to my research. I would like to also thank my instructors and graduate committee members at the University of Windsor who helped further my scientific knowledge. I am indebted to David Garfinkle at the department of physics at Oakland University for allowing me to refer to his code during the development phase. Without this reference many impediments would have slowed down the work. I am also very much obliged to my friends, all of whom have given me encouragement and have kept me sane throughout this work. To name a few: M. Cassar, A. Czajkowski, T. Harb, P. Ledwith, P. Liew, C. Magnuson and M. Tambasco, although there are many others who should be mentioned. I am especially thankful to Jennifer Babiak for encouragement and support without which this work would not have been possible.

Andrew DeBenedictis

1996

Table of Contents

Abstract	iv	
Dedication	v	
Acknowledgments	vi	
List of Figures	viii	
Notation	ix	
Chapter		
1	Gravitational Collapse	1
	Introduction	2
	Gravitational Collapse of the Scalar Field	4
	The Mass and Horizon Formulation	11
	The Double Null System	13
2	Computational Method	16
	Errors	23
3	Findings	26
	Numerical Testing	27
	Discrete Self-Similarity	29
	Black Hole Mass Scaling Law	31
	Gravitational Field Near the Origin	
4	Analysis	45
5	Concluding Remarks	52
	Appendices	55
	Appendix A: Derivation of Formulae	56
	Appendix B: Computer Code	65
	References	92
	Vita Auctoris	95

List of Figures

Figure

1	Incoming null geodesics	15
2	Test scalar field profile	35
3	Subcritical evolution of test profile	36
4	Supercritical evolution of test profile	36
5	Critical evolution of test profile	37
6	Fitted profiles at similarity times of test profile	37
7	Black hole scaling of test profile	38
8(a-d)	Form of $u=0$ scalar profiles	39
9(a-d)	Evolution of profiles	40
10(a-e)	Fitted profiles at similarity times	41
11(a-d)	Black hole scaling law	42
12	Ricci scalar near the origin	43
13	Light cone structure near the origin	44

Notation

The Einstein summation convention is used wherever there is an upper and lower repeated index unless otherwise specified. Latin indices can take on values 1, 2, 3 while Greek indices can take on the values 0, 1, 2, 3.

The four-dimensional Kronecker delta is written as

$$\delta^{\alpha}_{\nu} = \begin{cases} 1 & \text{if } \nu = \alpha \\ 0 & \text{if } \nu \neq \alpha \end{cases}$$

The sign of the metric, $g_{\mu\nu}$, is such that, unless otherwise specified, the metric on standard (unit) two spheres is strictly positive. The determinant of the metric is denoted by g .

The Ricci tensor is a contraction of the Riemann curvature tensor on the *first* and *third* indices. So that

$$R_{\mu\nu} = R^{\alpha}_{\mu\alpha\nu}$$

Units are such that the gravitational constant, G , and the speed of light, c , are both normalized to unity.

Partial derivatives are indicated by a comma such as

$$\frac{\partial f}{\partial x^{\mu}} = f_{,\mu}$$

while covariant derivatives are indicated by a semi-colon.

1. **Gravitational Collapse**

1.1. Introduction:

Large-scale gravitational collapse is found in nature in the study of stars. Because of the nature of the material medium (the fermions making up the star) and the initial dynamics, black holes formed by the gravitational collapse of a star will have a minimum mass; the Chandrasekhar mass. Equations governing such collapse are extremely complex making exact solutions prohibitive.

A simplified model which still allows one to study the general physics of gravitational collapse is that of a massless scalar field coupled to gravity. With the massless Klein-Gordon field as the material model, no stationary solutions are admitted and therefore there are only two possible outcomes for any initial data. These are: the formation of a black hole or alternately, evaporation where outgoing scalar radiation leaves behind a flat space-time. This property allows the formation of infinitesimal mass black holes. Numerical studies of scalar field collapse have been done for many years but, until recently, the fixed grid resolutions used have been too coarse to study the phenomena discussed here. Choptuik [1] carried out the first high precision numerical analysis of the region between the two outcomes using an adaptive mesh technique based on the Berger and Olinger algorithm [2]. Choptuik chose to scan a parameter p , some constant in the initial

scalar profile which governs the strength of gravity in the initial state. Two unexpected results were found from this study. It was found that if the parameter p was tuned to high precision to the critical parameter p^* (p^* corresponding to the formation of a null mass black hole) the critical solution displayed periodic discrete self similarity (DSS). That is, the field profile evolves to a copy of itself after a set period of time $\Delta_t \simeq e^{-3.43}$ and on a spatial scale $\Delta_r \simeq 30$ times smaller than the previous similar profile. There is an infinite series of echoes at $p = p^*$.

The second result occurs in the slightly *supercritical* case. In this case it is found that the mass of the black hole which forms follows the power law

$$M \sim (p - p^*)^\gamma, \tag{1.1}$$

where p is the value of the tuning parameter for the specific supercritical case, p^* is the critical parameter for the profile under study and γ is the critical exponent found by Choptuik to be universal and approximately equal to 0.37.

Other spherically symmetric studies done by Garfinkle [3], Hamade and Stewart [4] and others have found results similar to Choptuik's. A study of the complex scalar field by Hirschmann and Eardley [5] found a value of 26 for Δ_r . Hamade, Horne and Stewart [6] studied the critical collapse of an axion/dilaton system

occurring in string theory where the axion and dilaton make up the real and imaginary parts of a complex field respectively. In the axion/dilaton case a value for γ of 0.264 was obtained indicating that the value of γ may not be universal. A study of the axisymmetric collapse of gravitons by Abrahams and Evans [7] yielded a value of $e^{0.6}$ for $(\Delta_t)^{-1}$ and Δ_r . These latter studies seem to indicate that the phenomena occur independent of symmetries and the material medium. Hod and Piran [8] have recently suggested the existence of fine structure to the black hole scaling law as well as having done a study of the charged scalar field [9]. Studies of the phenomena in Brans-Dicke theory have also been done [10], [11]. Finally, analysis of the Choptuik problem was done by Price and Pullin [12] and an analysis of critical scalar field collapse was done by Gundlach [13].

1.2. Gravitational Collapse of the Scalar Field:

The Lagrangian density for the massless scalar field ϕ in the presence of gravitation is given by:

$$\mathcal{L} = \frac{1}{2} \sqrt{-g} (g^{\mu\nu} \phi_{,\mu} \phi_{,\nu}) . \quad (1.2)$$

From (1.2) both the wave equation,

$$\phi^{i\mu}{}_{;\mu} = 0 \tag{1.3}$$

and the stress-energy tensor for the scalar field,

$$T_{\mu\nu} = \phi_{,\mu}\phi_{,\nu} - \frac{1}{2}(g_{\mu\nu}\phi_{,\alpha}\phi^{,\alpha}) \tag{1.4}$$

can be derived. The conservation law

$$T^{\mu\nu}{}_{;\nu} = 0, \tag{1.5}$$

also implies the scalar wave equation (1.3).

We study the Einstein field equations

$$R_{\mu\nu} - \frac{1}{2}Rg_{\mu\nu} = 8\pi T_{\mu\nu} \tag{1.6}$$

where $T_{\mu\nu}$ is given by (1.4) and $g_{\mu\nu}$ is the spherically symmetric metric yielding the line element (in curvature coordinates):

$$ds^2 = -\alpha^2(t, r)dt^2 + a^2(t, r)dr^2 + r^2d\Omega^2. \tag{1.7}$$

Both α and a are functions of time and radius and the radial coordinate r is defined as a coordinate defining the area of metric two-spheres, S_2 , centered at $r = 0$,

$$Area(S_2) = 4\pi r^2. \quad (1.8)$$

Ω is the metric of the two-sphere, $d\Omega^2 = d\theta^2 + \sin^2(\theta) d\varphi^2$.

The non-zero Einstein equations expand to

$$\left(\frac{\alpha}{a} r^2 \phi_{,r}\right)_{,r} = r^2 \left(\frac{a}{\alpha} \phi_{,t}\right)_{,t} \quad (1.9)$$

$$\alpha_{,r} - \frac{\alpha}{a} a_{,r} = \left(\frac{a^2 - 1}{r}\right) \alpha \quad (1.10)$$

$$\frac{2}{a^2 r} \left(\frac{1}{\alpha} \alpha_{,r} + \frac{1}{a} a_{,r}\right) = 8\pi \left(\frac{1}{a^2} \phi_{,r} \phi_{,r} + \frac{1}{\alpha^2} \phi_{,t} \phi_{,t}\right) \quad (1.11)$$

$$\frac{4}{a^2 r} a_{,t} = 16\pi (\phi_{,r} \phi_{,t}). \quad (1.12)$$

We define the *mass function* by:

$$1 - \frac{2m}{r} = a^{-2} \quad (1.13)$$

so that the formation of a black hole is given by the condition

$$a^{-2} \rightarrow 0. \quad (1.14)$$

We now introduce a retarded time coordinate u as being a constant on future light cones of each point on a central world line (Bondi coordinates). In this coordinate system the metric (1.7) can be expressed as

$$ds^2 = - (e^{2v}) du^2 - 2 (e^{v+\lambda}) dudr + r^2 d\Omega^2 \quad (1.15)$$

and the wave equation(1.3) in full form reads:

$$-2 \left(\phi_{,u,r} + \frac{1}{r} \phi_{,u} \right) + e^{v-\lambda} \left[\phi_{,r,r} + \left(\frac{2}{r} + v_{,r} - \lambda_{,r} \right) \phi_{,r} \right] = 0. \quad (1.16)$$

Following convention [14], the function h is defined by:

$$h = \frac{\partial}{\partial r} (r\phi). \quad (1.17)$$

We also adopt the following notation: if f is a function of the coordinates (u and r , say), then \bar{f} is defined as the mean

$$\bar{f}(u, r) = \frac{1}{r} \int_0^r f(u, r') dr' \quad (1.18)$$

and therefore

$$f = \frac{\partial}{\partial r} (r\bar{f}) \quad (1.19)$$

implying that

$$\frac{\partial \bar{f}}{\partial r} = \left(\frac{f - \bar{f}}{r} \right). \quad (1.20)$$

Thus, from (1.17) and (1.19) we have:

$$\phi \equiv \bar{h}. \quad (1.21)$$

With this notation the non-zero Einstein equations (1.9-1.12) reduce to:

$$v_{,r} + \lambda_{,r} = 4\pi r \phi_{,r}^2 \quad (1.22)$$

admitting the solution

$$v + \lambda = -4\pi \int_r^\infty r' \phi_{,r'}^2 dr' \quad (1.23)$$

and

$$e_{,r}^{v-\lambda} = \frac{1}{r} (e^{v+\lambda} - e^{v-\lambda}) \quad (1.24)$$

with solution

$$e^{v-\lambda} = \frac{1}{r} \int_0^r e^{v+\lambda} dr'. \quad (1.25)$$

If we define

$$e^{v+\lambda} \equiv g, \quad (1.26)$$

then from (1.18) and (1.25),

$$\bar{g} = e^{v-\lambda}. \quad (1.27)$$

While, (1.20) and (1.23), give:

$$g = \exp \left[-4\pi \int_r^\infty \frac{1}{r'} (h - \bar{h})^2 dr' \right]. \quad (1.28)$$

Substituting g and \bar{g} in the metric (1.15) yields

$$ds^2 = -(g\bar{g}) du^2 - (2g) dudr + r^2 d\Omega^2 \quad (1.29)$$

and therefore the equation of an incoming null geodesic is given by:

$$\frac{\partial r}{\partial u} = -\frac{\bar{g}}{2}, \quad (1.30)$$

while the field equations become:

$$\frac{2}{r} \frac{g_{,r}}{g} = 8\pi (\bar{h}_{,r})^2 \quad (1.31)$$

and

$$\frac{2}{r^2} \bar{g} \left[\frac{g}{\bar{g}} + r \left(\frac{g_{,r} - \bar{g}_{,r}}{g} \right) - 1 \right] = 8\pi \bar{g} \bar{h}_{,r}^2. \quad (1.32)$$

The wave equation (1.16) along the incoming null geodesics becomes the nonlinear evolution equation for the scalar field

$$h_{,u} - \frac{1}{2} \bar{g} h_{,r} = \frac{1}{2r} (g - \bar{g}) (h - \bar{h}). \quad (1.33)$$

If we impose regularity at the origin and pick as a time coordinate the proper time of an observer at the origin (these conditions amount to $g(u, 0) = \bar{g}(u, 0) = 1$) then (1.33) ensures that the quantities $\bar{h} = \phi, v$ and λ solve the Einstein equations. This property along with the fact that the evolution is described along null geodesics

makes (1.33) the required equation to evolve the gravitational collapse of a scalar field in the null formulation used in this study.

1.3. The Mass and Horizon Formulation:

The mass dynamics are strongly related to the dynamics of the scalar field itself, $\phi \equiv \bar{h}$. The evolution of the quantity $r\bar{h}$ along incoming light rays (given by applying the differential operator of (1.33)) leads to the evolution law for \bar{h} if regularity at the centre is assumed (see Appendix A for derivation and proof),

$$\begin{aligned} (r\bar{h})_{,u} - \frac{1}{2}\bar{g}(r\bar{h})_{,r} &= -\frac{\bar{g}}{2}\bar{h} + \frac{1}{2}\int_0^r \frac{\bar{g}}{r}(h - \bar{h}) dr \\ \Rightarrow \bar{h}_{,u} - \frac{1}{2}\bar{g}\bar{h}_{,r} &= \frac{1}{2r}\int_0^r \frac{\bar{g}}{r}(h - \bar{h}) dr. \end{aligned} \quad (1.34)$$

The mass function (1.13) can be re-written in terms of the new variables as:

$$m = \frac{r}{2} \left(1 - \frac{\bar{g}}{g} \right), \quad (1.35)$$

where m gives the total mass enclosed within a sphere of radius r at retarded time u while the expression for the radial mass-energy density,

$$m_{,r} = 2\pi \frac{\bar{g}}{g} (h - \bar{h})^2, \quad (1.36)$$

allows us to write

$$m = 2\pi \int_0^r \frac{\bar{g}}{g} (h - \bar{h})^2 dr. \quad (1.37)$$

While the field equations give us (in terms of m),

$$m_{,u} - \frac{1}{2}g(m)_{,r} = 4\pi r^2 \left[\frac{1}{2r} \int_0^r \frac{\bar{g}}{r} (h - \bar{h}) dr \right]^2. \quad (1.38)$$

This equation gives the evolution of the mass function (the left-hand-side) in terms of the evolution of the scalar field (1.34) (bracketed term on the right-hand-side). The total mass over all space $\left(\lim_{r \rightarrow \infty} m(u, r) \right)$, is the Bondi mass. The mass evolution equation (1.38) implies Bondi's theorem.

Condition (1.14) for horizon formation translates to the condition:

$$\frac{\bar{g}}{g} \rightarrow 0 \quad (1.39)$$

(from (1.35)) although the exact condition cannot be checked numerically (more on this in chapter two).

1.4. The Double Null System:

There are advantages in implementing the use of double null coordinates. For example, the problem of increasing the spatial resolution to track the shrinking spatial features can be overcome by "tying" the radial grid points to incoming null geodesics (see fig.1). As time evolves (by an amount Δ_t , say), the spatial features shrink (by a factor Δ_r), but the overall size of the grid as well as the grid spacings also shrink as the grid points evolve along the incoming light rays. This way the resolution is maintained. The double null coordinates, u and v are defined to be constant on conjugate light rays.

In the transformation to double null coordinates, the radial coordinate, r , becomes a function of the new coordinates,

$$r \equiv r(u, v), \tag{1.40}$$

and therefore we define

$$dr = \frac{\partial r}{\partial v} dv. \tag{1.41}$$

Then the line element becomes:

$$ds^2 = -\Sigma^2 dudv + r^2 d\Omega^2. \quad (1.42)$$

Where

$$\Sigma^2 \equiv 2g \frac{\partial r(u, v)}{\partial v}, \quad (1.43)$$

and g is the same function as in the last section.

The Einstein-scalar field equations become:

$$\frac{2}{\Sigma r} r_{,u} \Sigma_{,u} - \frac{r_{,u,u}}{r} - (\phi_{,u})^2 = 0 \quad (1.44)$$

$$\frac{2}{\Sigma r} r_{,v} \Sigma_{,v} - \frac{r_{,v,v}}{r} - (\phi_{,v})^2 = 0 \quad (1.45)$$

$$\phi_{,u,v} + \frac{r_{,u} \phi_{,v}}{r} + \frac{\phi_{,u} r_{,v}}{r} = 0 \quad (1.46)$$

$$r_{,u,v} + \frac{r_{,u} r_{,v}}{r} + \frac{1}{4r} \Sigma^2 = 0. \quad (1.47)$$

The evolution equations from the last section retain their form with the slight modifications (1.40) and (1.41). For example, a function \bar{f} is defined as (cf. (1.18))

$$\bar{f} \equiv \frac{1}{r} \int_0^v f(u, v') \frac{\partial r(u, v')}{\partial v'} dv'. \quad (1.48)$$

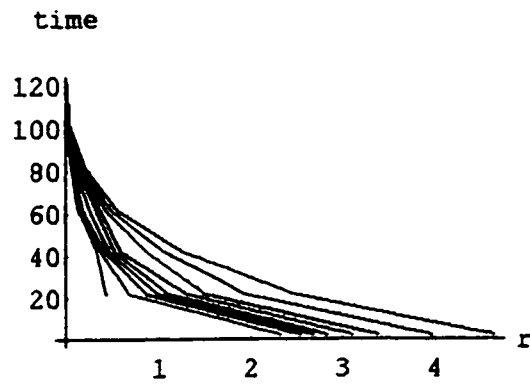


Fig.1: The evolution of inward null geodesics. The system is probed on the incoming light rays to increase resolution as time evolves.

2. **Computational Method**

The basic code involves a grid construct in space-time. For reasons which will become apparent, we chose to study the behaviour of the dynamic quantity h . Therefore, the value of h on the $u = 0$ surface is the initial data for the Einstein-scalar field equations. The initial data is probed at optimum radii determined by an adaptive quadrature technique based on Simpson's rule.

The adaptive quadrature technique works as follows. The quantity

$$s = \int_a^b h dr \quad (2.1)$$

is evaluated using a form of Simpson's rule:

$$s \approx \frac{1}{6} \sum_{i=0}^N \frac{b-a}{N} [h(r_i) + 4h(r) + h(r_{i+1})], \quad (2.2)$$

where $r_0 = a$, $r_N = b$, N is the number of intervals the function is split into and r in the middle bracketed term is $\frac{r_i+r_{i+1}}{2}$. Initially, the limits are $a = 0$ and $b = r_{\max}$, some maximum radius which encompasses the bulk of h and \bar{h} . The program evaluates s for $N = 10$ and $N = 5$. If the difference is greater than some user defined tolerance the program will evaluate

$$s = \int_a^{\frac{a+b}{2}} h dr + \int_{\frac{a+b}{2}}^b h dr \quad (2.3)$$

using (2.2). Again, each part of (2.3) is evaluated with $N = 10$ and $N = 5$ and the difference is compared to the tolerance. The process is repeated until all sections are evaluated within the tolerance. With this technique, sections of s with large curvature are sampled at more radii than sections with little curvature providing optimum resolution on the initial data.

A difficulty arises in the double null technique where resolution can become too coarse too quickly to study the spatial structure. This is due to the fact that the null geodesic corresponding to the outermost grid point does not evolve to a value close enough to the origin to maintain the required resolution (resolution is generally maintained for at least some part of the run before being lost). There is no apriori way to know if resolution has been maintained throughout the run and therefore most of the run must be executed and the data analyzed before this problem can be detected. To overcome this one can, to some extent, change the value of r_{\max} in the initial data. One ideally does not want the light ray corresponding to r_{\max} to hit the origin before the features have evolved. Also, the light ray should not be too far out so that small features cannot be resolved by

the end of the evolution.

The motivation for using the adaptive technique is the following. Another way to overcome the resolution problem is to increase the number of grid points. By decreasing the value of the tolerance, one can arbitrarily (to machine limit) increase the number of grid points. The initial grid points are positioned at optimum radii for the initial data. However, the DSS condition,

$$h(r, t) = h(r\Delta r, t + \Delta t), \quad (2.4)$$

ensures that the data never departs drastically from the initial conditions.

Since the grid points are tied to the incoming light rays, the number of grid points decreases as the light rays hit the origin during the evolution. To overcome this problem a technique similar to that used in [3] is utilized.. In [3] the evolution was allowed to proceed until half of the grid points were lost. These grid points were then placed in between each of the remaining grid points to maintain resolution. Here this procedure has been slightly modified in that the number of grid points which have to vanish before re-introduction is allowed to vary for each run. In practice, it was found that there is little advantage in keeping this number small since the run takes considerably longer if the code is constantly

re-introducing grid points.

Inaccuracies occur near the origin in quantities where one divides by r . This is overcome by first expanding h in the Taylor series;

$$h = h_0 + h_1 r + O(r^2). \quad (2.5)$$

Using this definition for h , the quantities \bar{h} , g and \bar{g} are given respectively by:

$$\bar{h} = h_0 + \frac{1}{2}h_1 r, \quad (2.6)$$

$$g = 1 + \frac{\pi}{2}h_1^2 r^2 + O(r^4), \quad (2.7)$$

$$\bar{g} = 1 + \frac{\pi}{6}h_1^2 r^2, \quad (2.8)$$

where (2.7) is itself a Taylor series in r . The above formulae are used for the first three radii from the origin while Simpson's rule for unequally spaced partitions is used for all other radii. The value of h_1 is found by fitting the first four values of h to a line where h_0 is the first h value.

The program requires the user to supply a value for the location of the outermost grid point (r_{\max}) on the initial data surface as well as a maximum and minimum value for p where the maximum value is supercritical and the minimum

value is subcritical. Next the quantities h , \bar{h} , g and \bar{g} are calculated and then evolved one step forward in time and the location of the grid points are evolved along the fronts of incoming light rays according to (1.30). The time step, du , is compared to the change in radii and is set so that the change in null geodesic r_k is less than a quarter the distance between it and a null geodesic r_{k-1} . That is,

$$du < \frac{r_k - r_{k-1}}{2\bar{g}}. \quad (2.9)$$

The program continues until either full evaporation or black hole formation occurs. The critical parameter is found utilizing a binary search technique, initially using p_{max} and p_{min} , based on whether or not a black hole forms.

The formation of a black hole is monitored by the behaviour of the quantity \bar{g} , with the vanishing of this quantity corresponding to horizon formation. The condition requiring regularity at the origin ($g_{r=0} = \bar{g}_{r=0} = 1$) causes g to diverge on the horizon as well as the divergence of \bar{g} on the corresponding null geodesic. Therefore, black hole formation is inferred by checking the divergence of the functions.

To study the DSS phenomena the code was executed by first analyzing the initial profiles of h and \bar{h} . The outermost grid point was chosen so that the grid

samples the bulk of the initial features. The tolerance was picked so that no more than 500 grid points were used. This limit is due to machine speed and memory. The code was then run until the critical parameter was determined to machine precision ($\frac{\delta p}{p} = 10^{-16}$). Analysis of the data then allows for a refined estimate of the outermost grid point and a refinement of the tolerance. After a few runs, the parameters will be found yielding resolution that is almost adequate. At this point, the changes in the parameters should be slight as drastic changes will alter the initial conditions and subsequent dynamics to an extent that may worsen the final resolution. Eventually, the outermost grid point is chosen so that it evolves close enough to the singularity as to maintain adequate resolution but without hitting the origin.

Next, the code was run to determine the scaling law of the mass of the black hole. The code was run at supercritical values of p to form various mass black holes. The double null technique is not very well suited for the study of the scaling law since here one is treating a range of supercritical p and the outermost grid point must not hit the origin during each of these evolutions. However, as p approaches p^* the outermost grid point may be too far out to resolve features corresponding to black hole formation. There is therefore only a limited range of p that can be scanned reliably using this technique.

2.1. Errors:

The technique used here, like all numerical techniques, is subject to a number of errors. As previously mentioned, there are limits in accuracy due to the machine floating point capability. There is a limit as to how close one can tune to the critical parameter. Ideally one would like to critically evolve the system such that the mass of the black hole which forms is as close to null as possible. In practice, critical parameter precision to 10^{-16} generally generates black hole masses of the order of 10^{-5} . This means that only a limited number of echoes can be created before either horizon formation occurs or evaporation disperses the field.

Another source of error comes from treating a continuous evolution in a finite number of steps. One can gain greater accuracy by decreasing the tolerance to arbitrarily small, however this would be at the great expense of speed. To insure that evolution steps are not too drastic the change in all probe radii is monitored during each evolution step and is kept sufficiently small by condition (2.9).

As described earlier, quantities near the origin are based on the expansion of h to order r . If the first few probe radii are sufficiently small this expansion should be sufficient. Obviously the radii are at their largest at the start of the evolution and therefore checking the first three radii at $u = 0$ is a good indication

of the accuracy of this expansion. For greater accuracy one could allow the code to evolve the system with exact solutions of h until the values of r near the origin become smaller than some value. After this point the evolution would proceed via the Taylor expansion.

With the null technique used here one runs into the problem of having to re-introduce grid points to the system. Once a grid point hits the origin it must eventually be replaced somewhere in the evolution to ensure adequate resolution. The problem is what value for h do we assign to this new point. After redefining the array to accept the new grid points, the new points are given a value equal to the average value of its adjacent grid points. That is,

$$h_i(r_{new}) = \frac{1}{2} (h_{i-1}(r_{new}) + h_{i+1}(r_{new})) \quad (2.10)$$

giving a maximum error in this new point of

$$\delta(h_i(r_{new})) = \frac{|h_{i-1}(r_{new}) - h_{i+1}(r_{new})|}{2}. \quad (2.11)$$

A better solution would certainly be to introduce an enormous number of gridpoints at the beginning of the evolution and accept the losses as these points

hit the origin. The enormous number of grid points required for such a scheme make this solution unfeasible given present computing power.

3. Findings

3.1. Numerical Testing:

In order to test the code, an initial "open" Gaussian test profile was used,

$$\phi(0, v) \equiv \bar{h}(0, v) = \frac{3\phi_0}{2r} \left\{ \begin{array}{l} \left[\frac{r_0(1-\sigma^2)}{e^{r_0^2/\sigma^2}} \right] + \frac{(r_0\sigma^2 - r_0 - r + \sigma^2 r + \frac{2}{3}r^3)}{e^{\frac{(r-r_0)^2}{\sigma^2}}} \\ + \frac{\sqrt{\pi}(1-\sigma^2)(2r_0^2 + \sigma^2)}{2\sigma} (\text{Erf} \left[\frac{r_0}{\sigma} \right] + \text{Erf} \left[\frac{r-r_0}{\sigma} \right]) \end{array} \right\}, \quad (3.1)$$

where r_0 and σ are fixed and ϕ_0 is the parameter treated as p . Erf is the error function,

$$\text{Erf}[x] \equiv \frac{2}{\sqrt{\pi}} \int_0^x e^{-t^2} dt. \quad (3.2)$$

The reason for choosing such a profile is that the critical behaviour of this initial data has been studied in [3] and therefore comparison of the results will provide a test for the code used here. The results obtained here are in agreement with those of Garfinkle verifying that the code does work. This test profile is shown in figure 2.

As discussed earlier, the evolution of (3.1) has two possible outcomes: evaporation or black hole formation. This data was evolved at subcritical and supercritical respectively to produce figures 3 and 4. These figures are plots of the function

h (vertical axis) and increase in time as one moves towards the back of the plot. It can be seen in the subcritical case that after some initial evolution the scalar field becomes trivial while the formation of a black hole can be seen near the back of the supercritical plot. The spatial and temporal axes of the three dimensional plots are not immediately meaningful. The scale on the radial axis increases as one goes forward in time since the sample points move along the null geodesics. The "bump" corresponding to black hole formation in figure 4 is therefore magnified by a factor $\approx 30^2$ compared to the front of the plot (if the scale were constant this bump would be a spike too thin to be plotted). The time axis represents time skips (in terms of proper time at the origin) but, because of condition (2.9), the increments are unequal.

The data was then evolved at criticality. The function h at $p = p^*$ is shown in figure 5. After some initial evolution the scalar field settles to a periodic behaviour. To examine self similarity, the regions where h is a maximum at $r = 0$ are plotted together in figure 6. These plots were constructed by plotting the first maxima and then multiplying subsequent maxima by a magnification factor, Δ_r , so that the deviation between the plots is minimal. For this data a value of $\Delta_r = 33.5$ for the second data set and $\Delta_r = 34^2$ for the third data set provided the graph. These results are in agreement with Choptuik's [1].

If u^* is defined as the value of u when the singularity forms, we then define:

$$T \equiv -\ln(u^* - u), \quad (3.3)$$

and use this as our measure of time. The plots in figure 6 correspond to T values of 2.59, 6.04, and 9.51. These times are equally spaced with an average spacing of $\Delta T \equiv -\ln(\Delta_t) = 3.46$. These results are also in agreement with [1].

The data was then evolved for a series of $\phi_0 > p^*$ to study the black hole mass scaling law. As mentioned earlier, p cannot deviate greatly from p^* limiting the mass range that can be studied. The results, along with a fitted curve are shown in figure 7. The equation of the fitted curve is

$$M = 3.025 (p - p^*)^{0.375}. \quad (3.4)$$

The value of 0.375 for the exponent, γ , agrees with Choptuik's results.

3.2. Discrete Self-Similarity:

To show that the phenomena are universal, four different initial profiles (plus the test profile above) are evolved in this study. These families are listed in table 1 along with the parameter used as the parameter p .

Profile	Form of $u = 0$ data	p
a)	$\phi_0 r^2 \exp \left[- \left(\frac{r-r_0}{\sigma} \right)^2 \right]$	ϕ_0
b)	$\phi_0 r^3 \exp [-3(r - r_0)]$	ϕ_0
c)	$\phi_0 \tanh \left[\left(\frac{r}{\sigma} \right)^q \right]$	ϕ_0
d)	$\phi_0 r^2 \left\{ \left[\exp \left(\frac{r-r_0}{\sigma} \right) - 1 \right]^{-1} + Ar \exp \left[- \left(\frac{r-r_1}{\sigma} \right)^2 \right] \right\}$	ϕ_0

These profiles are shown in figures 8 (a-d) (solid) along with their radial mass-energy density, m_r given by (1.36) (dots).

These initial profiles were run until the critical parameter was achieved to machine precision. The evolution of these profiles is shown in figures 9 (a-d) where the axes should be interpreted as described in the previous section. In profile c) it can be seen that the evolution is too far subcritical and goes to zero shortly after the second maximum. A value for the critical parameter could not be obtained within machine precision which would yield a solution closer to criticality for this profile. As with the test profile, regions where h is a maximum at the origin were picked and plotted together for each profile in figures 10 (a-e). Figure 10e shows regions for profile d) where $h = 0$ at the origin. Again a value of Δ_r was picked which minimizes the deviation between the family of curves. These results are tabulated in the figure captions along with the time, T , corresponding

to each plot and average ΔT . The similarity of these values strongly suggests data independence. The average ΔT , taking all profiles into account is found to be ≈ 3.45 ($\Delta_t \approx 0.0317$) while the average Δ_r is ≈ 31.4 .

3.3. Black Hole Mass Scaling Law:

Each profile from table 1 was evolved with various supercritical values of p to create black holes of varying mass. Figures 11 (a-d) show the black hole mass as a function of p (dots) along with a best fit curve (solid) of the form

$$M = k(p - p^*)^\gamma. \quad (3.5)$$

The value of k and the critical exponent, γ , for each plot is given in the figure captions. It can be seen that although k varies for different initial data, γ is approximately equal for each profile and therefore apparently universal for real massless scalar fields. The value, averaged over all profiles, is $\gamma \approx 0.364$. It has been mentioned, [15], that this number is very close to the value of $1/e \approx 0.367$ although at this time no arguments can be made requiring the critical exponent to have the value $1/e$.

3.4. Gravitational Field Near the Origin:

The nature of the scalar field allows the creation of high curvature regions in small areas of the space-time. A natural question which arises is how long does it take for information from areas of extreme curvature to reach a distant observer. At super-critical and barely subcritical, areas of highest curvature occur near the origin after some evolution time. Near the origin, the Ricci curvature scalar is given by (see Appendix A)

$$R_{r \rightarrow 0} \approx 2\pi h_1^2, \quad (3.6)$$

where h_1 is the same quantity described earlier. A plot of (3.6) as a function of time is shown in figure 12 for profile d) at slightly subcritical ($p = p^* - 10^{-15}$). The time axis should be interpreted as in earlier graphs. The oscillatory behaviour due to the DSS phenomena is apparent along with evaporation towards the right of the graph. It can be seen that the curvature becomes very large sometime during the evolution as would be expected for near critical collapse.

An argument by Hamdé and Stewart [4] goes as follows. Study two evolutions of the same initial profile with one evolution being slightly subcritical and one being slightly supercritical ($\delta p = \epsilon$, with $\epsilon \ll 1$). Initially, the two solutions will

evolve almost identically due to the similarity of the initial data. Bifurcation must occur by late time however since one data set forms a black hole whereas the other disperses. By continuity arguments, as $\epsilon \rightarrow 0$ the time required for a subcritical photon to reach the distant observer should become very large.

Calculations here and in [4] (who used a variation of the Berger-Oliger adaptive mesh technique) suggest the opposite. The light cone structure near the origin for profile d) is shown in figures 13 (a-b) with initial conditions identical to those which produced figure 12. Each dot corresponds to an outgoing light ray starting near the origin sometime during the period of maximum curvature (the time period corresponding to the largest "bump" in figure 12). It can be seen that as time evolves, the outgoing null geodesics develop *shallower* slopes. The opposite of what one gets with black hole formation. A distant observer need only wait a finite proper time to see subcritical strong field regions, even for conditions arbitrarily close to critical.

The double null technique is not well suited for the above study and therefore an explanation of how figures 13 a) and 13 b) are constructed is in order. Since the radii are tied to the incoming null geodesics, quantities such as \bar{g} (a quantity which is required to evolve light cones via (1.30)) are also evaluated at the incoming positions. If one picks a starting position, r_0 , near the origin and wishes to evolve

this position *outward* a step in time du according to (1.30), \bar{g} at r_0 can be used. Now a point at $r = r_0$ at a later time is required for evolution. The problem is that since the radii have evolved inward, there is no guarantee that a point at r_0 , and therefore $\bar{g}(r_0)$, is present at this new time. A second problem comes from the fact that the size of the time steps are governed by (2.9) and therefore a null line at time u_1 may be evolved a different amount of time than a null line at time u_2 .

The first problem can be overcome by evolving the initial data at a low value of the tolerance. This way, there are a large number of grid points and the density of these grid points is large at late times. To produce figures 13 a) and b) points at different times during high curvature were found which agree within 10^{-5} of each other. These points were singled out and used as r_0 and evolved some time along outward null geodesics. The change in r was then divided by the change in time to reduce the problem due to different time skips. Thus, figures 13 a) and 13 b) are plots of $\Delta r / \Delta u$ for outgoing light rays near the origin.

scalar field

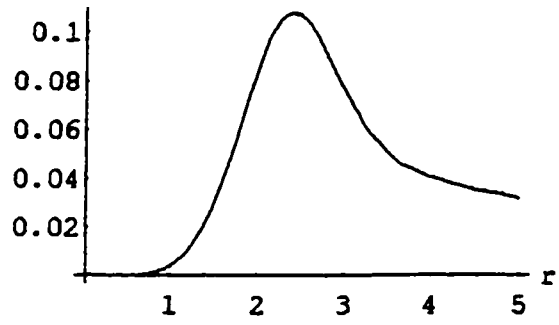


Fig 2: The test profile at $u = 0$.

Fig.3

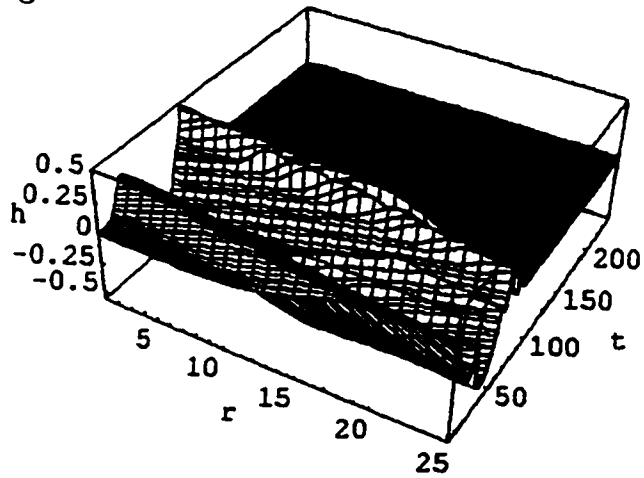


Fig.4

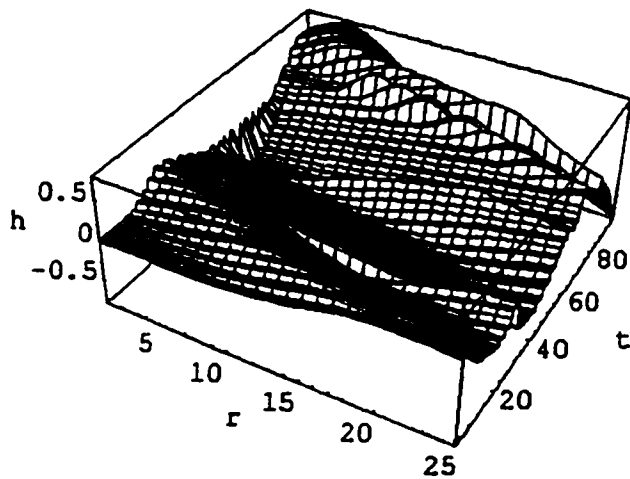


Fig. 3 and 4: Subcritical and supercritical evolutions of h for the test profile. Note evaporation in the subcritical case as one progresses in time. Also note the horizon formation (bump) near the rear of the supercritical case. See main text for details about the plot axes.

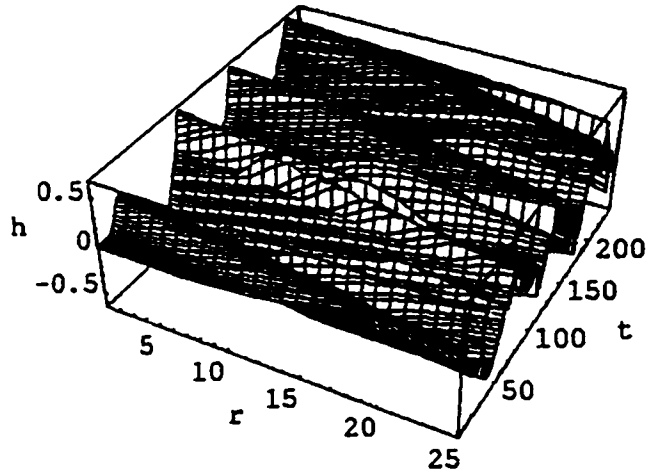


Fig. 5: Critical evolution of h for the test profile. Notice that after some initial evolution the behaviour becomes periodic.

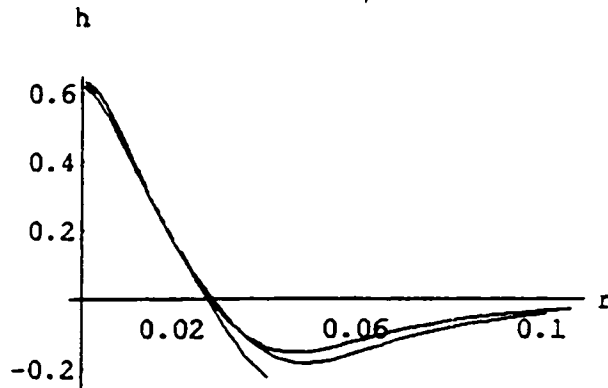


Fig. 6: Fitted profiles of h where fig 5 is a maximum at the origin. The second maxima in fig. 5 is magnified by a factor of 33.5 while the third maxima is magnified by a factor of 34^2 .

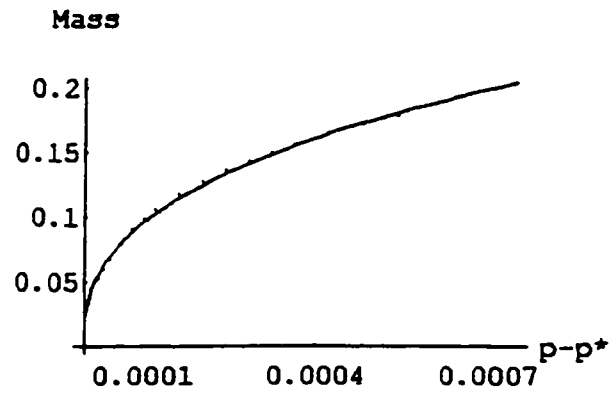


Fig. 7: Black hole masses at supercritical. The dots represent masses of black holes which formed at supercritical p while the solid curve is that of equation (3.4).

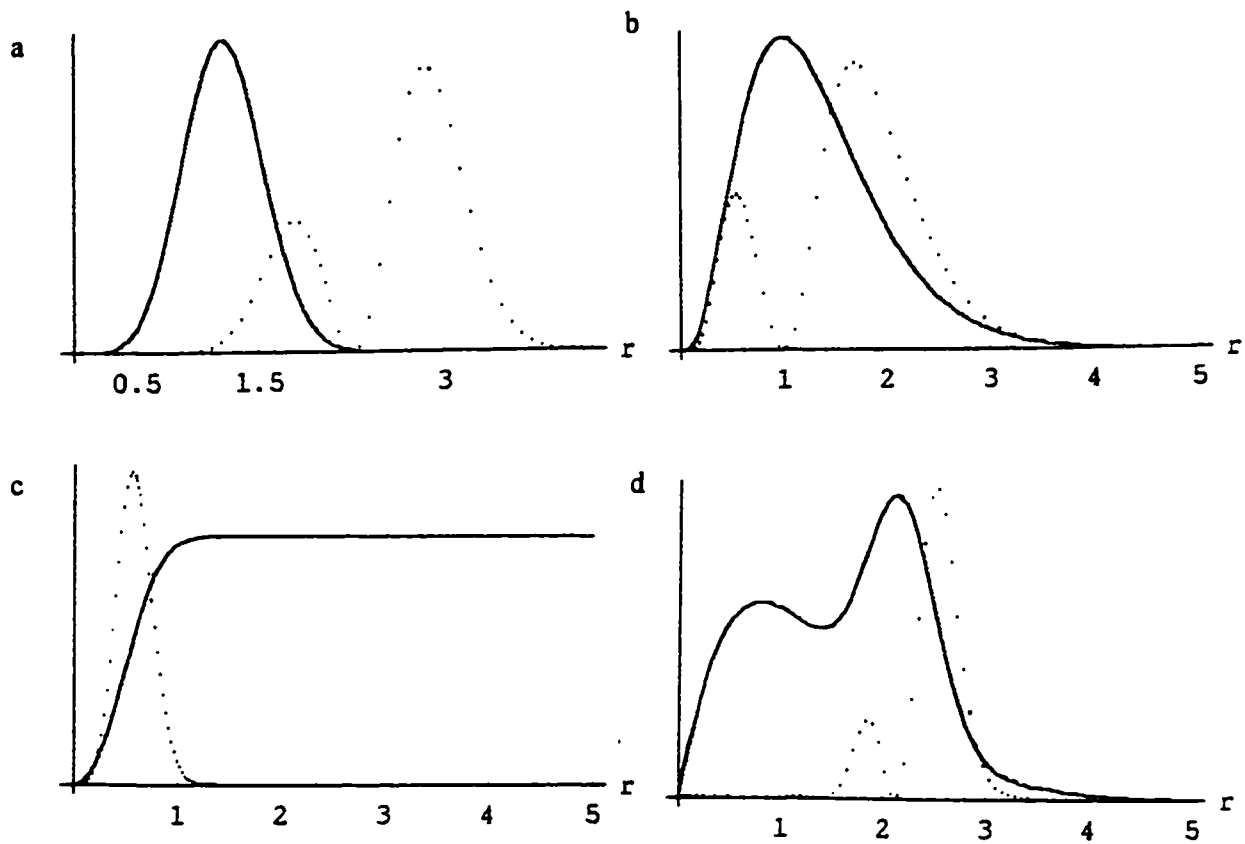


Fig. 8 (a-d): Form of initial data, ϕ , (solid) along with radial mass-energy density (dots) for families a-d.

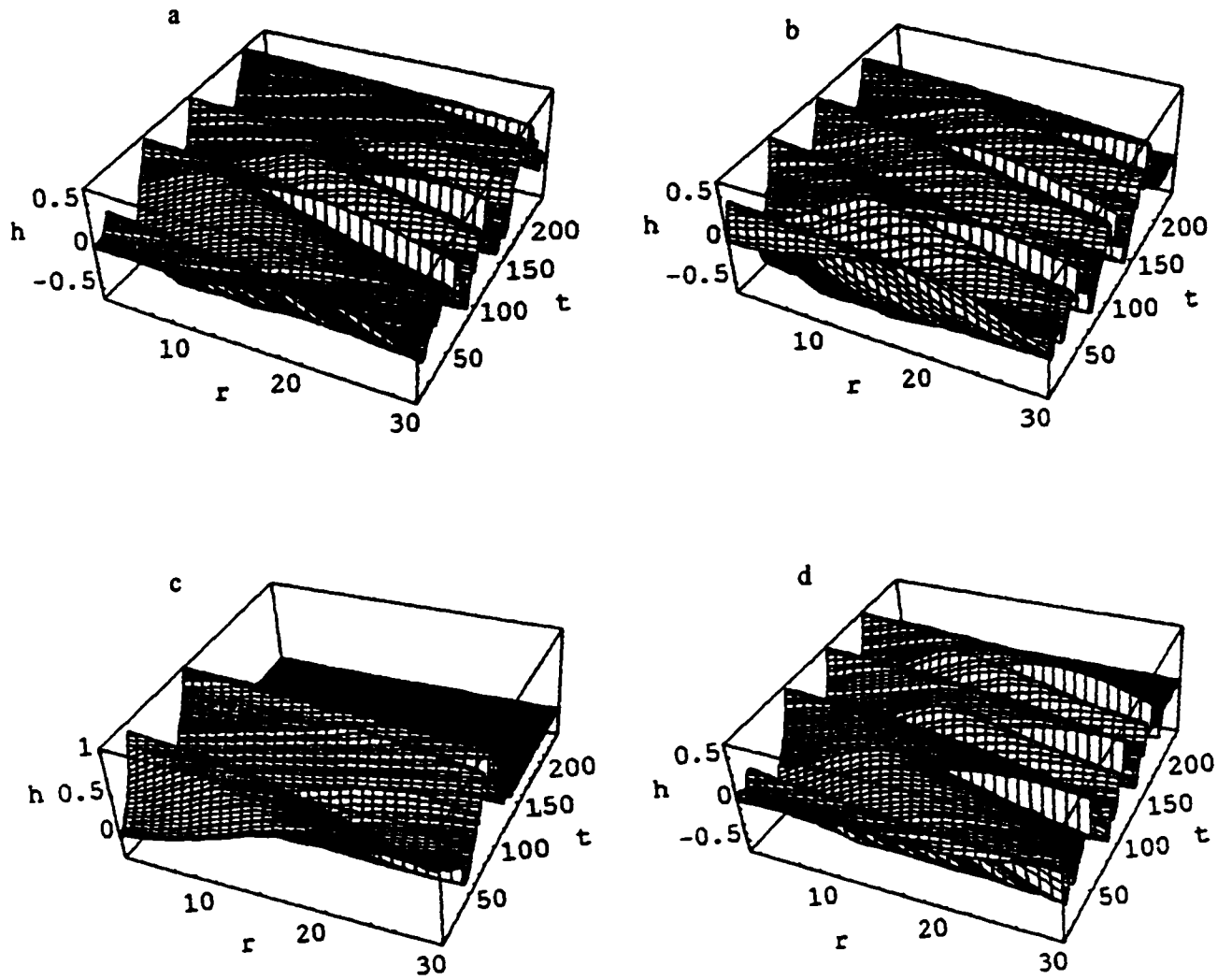


Fig. 9 (a-d): Evolution of Profiles a-d at criticality. Note in c that the evolution is slightly too subcritical so that the field has dispersed near the back of the plot.

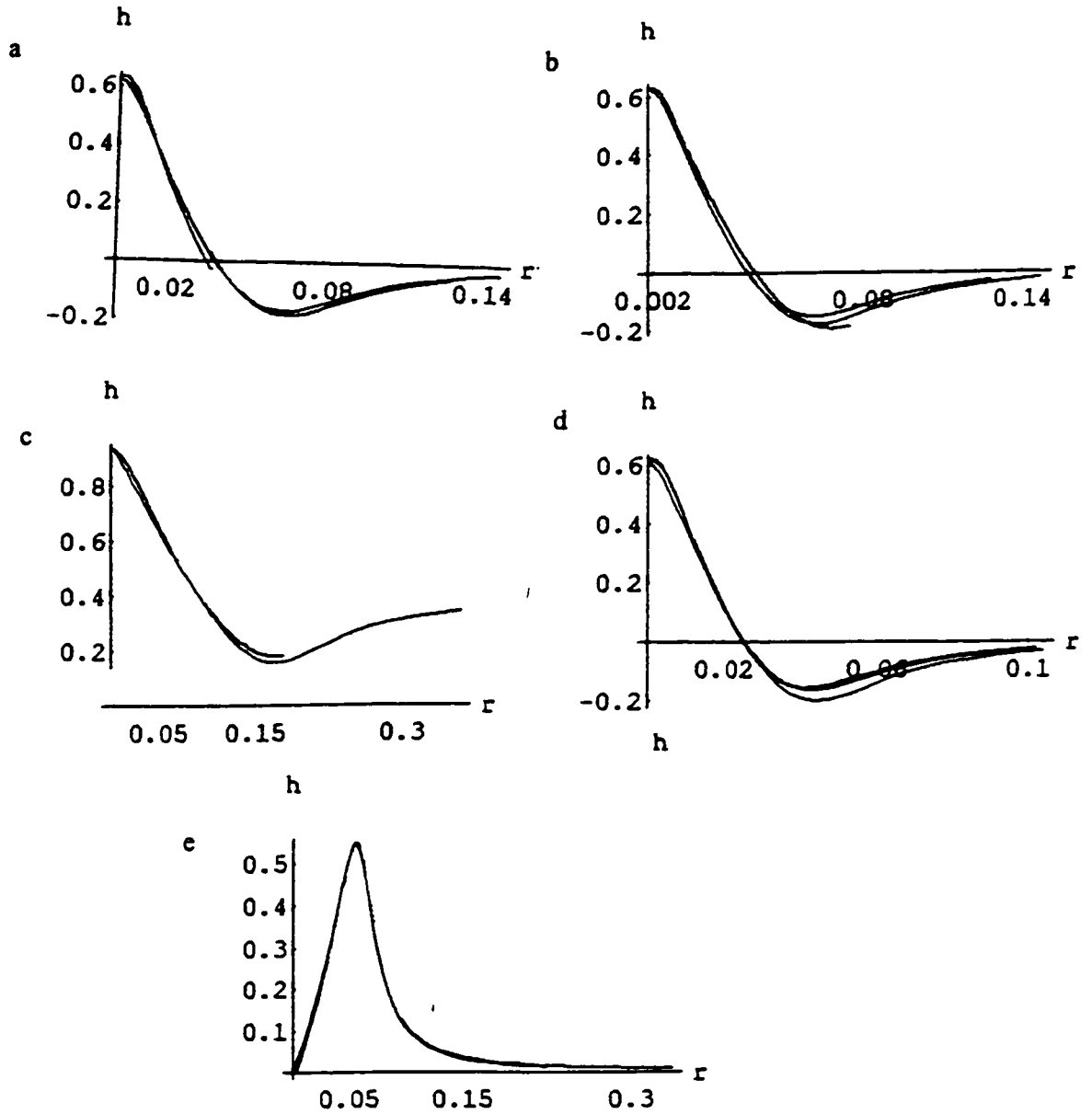


Fig. 10: Fitted profiles. Similarity times for profile a) are $T = 2.47$, $T = 5.91$, $T = 9.43$ giving an average ΔT of 3.48. For profile b) $T = 2.39$, $T = 5.84$, $T = 9.33$ giving an average ΔT of 3.47. For profile c) $T = 2.11$, $T = 5.57$ giving an average ΔT of 3.46. For profile d) $T = 2.51$, $T = 5.98$, $T = 9.37$ giving an average ΔT of 3.43. The last figure displays fitted profiles for scalar field d with $h = 0$ at $r = 0$. For this case $T = 1.70$, $T = 5.14$, $T = 8.53$ giving an average ΔT of 3.42. Magnification factors are as follows: a) $\Delta_r = 33.5$ and 30^2 . b) $\Delta_r = 28$ and 33^2 . c) $\Delta_r = 29.5$. d) $\Delta_r = 30$ and 34^2 . e) $\Delta_r = 32.5$ and $(32.5)^2$.

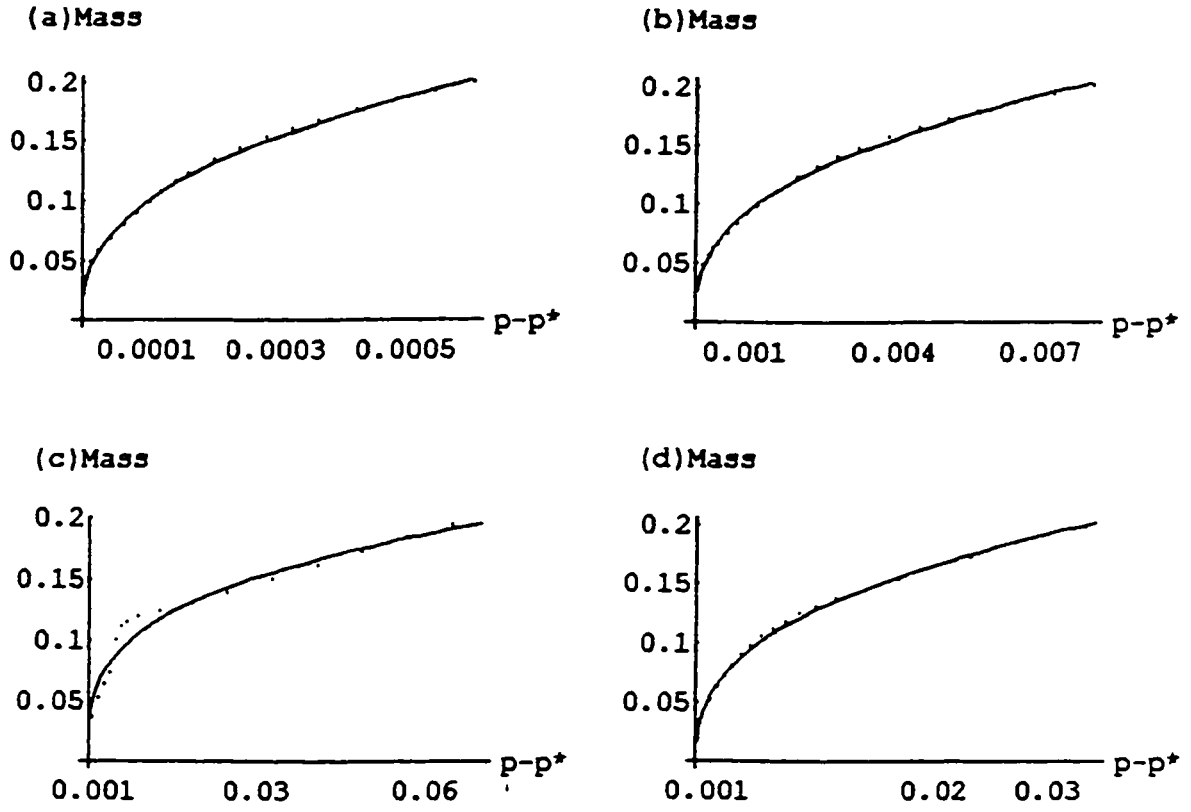


Fig. 11 (a-d): Black Hole masses (dots) for profiles a-d along with best fit curves. For profile a) $\kappa = 3.803$, $\gamma = 0.396$. For profile b) $\kappa = 1.279$, $\gamma = 0.381$. For profile c) $\kappa = 0.439$, $\gamma = 0.303$. For profile d) $\kappa = 0.724$, $\gamma = 0.377$.

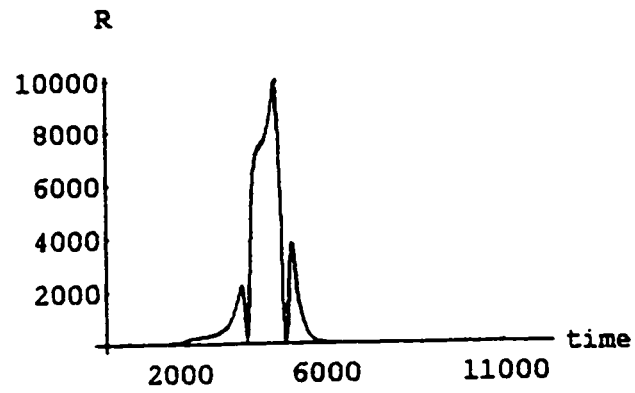


Fig. 12: Ricci curvature scalar, R , near the origin at marginally sub-critical. Note the periodic nature due to the behaviour of the metric functions.

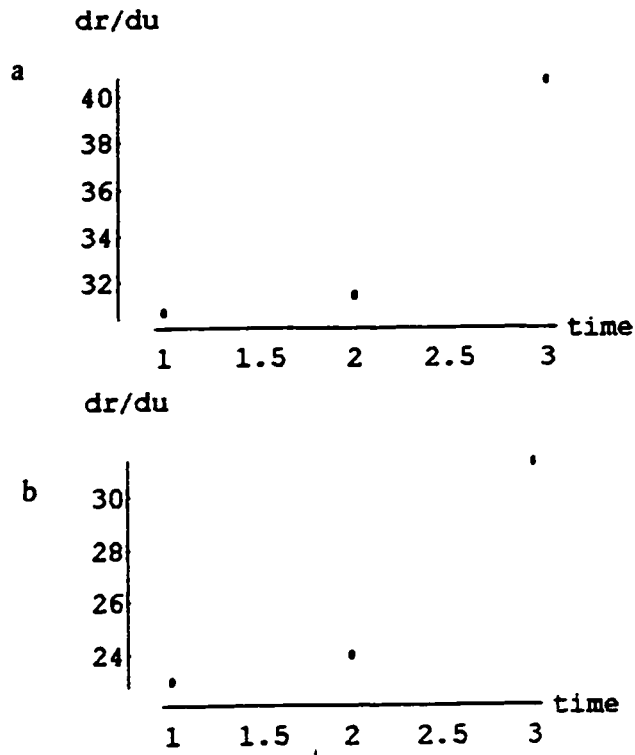


Fig. 13 (a-b): Light cone structure near the origin at marginally sub-critical during a period of high curvature. Note that the value of dr/du gets larger indicating a shallower light cone as time progresses. Each figure was generated using a different starting point near the origin (see main text).

4.

Analysis

There is no simple explanation for any of the above results. The apparent universality which this study shows of the phenomena seems to suggest that scalar field collapse may be governed by a single solution to the Einstein-scalar field equations. Analysis can be simplified by making the following assumptions. The first is the assumption of continuous self-similarity (CSS). From the previous section it can be seen that the period between successive echoes becomes shorter by the factor Δ_t and therefore the CSS assumption becomes acceptable after a certain number of echoes. Note that $\Delta_t \approx \frac{1}{\Delta_r}$ and therefore a time coordinate (assuming CSS) should exist such that metric components depend on a quantity $x = r/u$ where u is the retarded time coordinate. Further, it is assumed that the space-time admits a vector field, ξ , such that the metric obeys

$$L_\xi g_{\mu\nu} = 2g_{\mu\nu}, \tag{4.1}$$

where L_ξ is the Lie derivative with respect to ξ . Such a space-time is known as homothetic. The interested reader is referred to [16] for a detailed study of homothetic scalar field collapse assuming CSS. The scalar field evolution equation in such a space-time becomes

$$\phi = \bar{h}(r/|u|) - \kappa \ln |u|. \quad (4.2)$$

One can immediately see that the parameter κ plays a role analogous to the parameter p . The self-similar Einstein-scalar field equations are:

$$(xg)_{,x} = g, \quad (4.3)$$

$$xg_{,x} = 4\pi g\gamma^2, \quad (4.4)$$

$$g - \bar{g} = 4\pi [2\kappa^2 x - (\bar{g} - 2x) (\gamma^2 + 2\kappa\gamma)], \quad (4.5)$$

where g and \bar{g} are the same functions described in earlier chapters. γ is a function such that

$$\bar{h}(x) = \int_0^x \frac{\gamma(\xi)}{\xi} d\xi. \quad (4.6)$$

Solutions to differential equations of the form (4.3-4.5) are given in [16] (although there are other CSS studies) and therefore will only be summarized here.

The subcritical solutions are characterized by $\kappa^2 \geq 1/4\pi$ while κ^2 slightly less than $1/4\pi$ permit some solutions with naked singularities. A transition between

black holes (here the term black hole simply refers to space-times with an apparent horizon) and naked singularities occurs in this regime. It is obvious from this discussion that the critical point, described by p^* , corresponds to the CSS case where $\kappa = 1/4\pi$.

The self similar space-times such as those described here do not allow for black holes with finite mass. One must therefore end the self-similar evolution at some time and match it to a less similar exterior. The existence of naked singularities in such a scheme may be supported by the behaviour of the light cone structure near the origin as obtained in the previous chapter.

Creating a discretely self-similar solution is more difficult. In DSS symmetry there can exist a ψ and constant Δ satisfying the condition

$$(\psi_*)^n g_{\mu\nu} = e^{2n\Delta} g_{\mu\nu}, \quad (4.7)$$

where n is any integer and ψ_* is the pull back of the diffeomorphism ψ . A solution in just such a space-time is constructed in [13]. Coordinates σ and x^a are chosen so that a point at $p = (\sigma, x^a)$ will have coordinates $(\sigma + \Delta, x^a)$ under the action of $\psi(p)$. This gives the metric the following property:

$$g_{\mu\nu}(\sigma, x^a) = e^{2\sigma} \hat{g}_{\mu\nu}(\sigma, x^a), \quad (4.8)$$

where $\hat{g}_{\mu\nu}$ satisfies

$$\hat{g}_{\mu\nu}(\sigma, x^a) = \hat{g}_{\mu\nu}(\sigma + \Delta, x^a). \quad (4.9)$$

If a vector field $\chi \equiv \partial/\partial\psi$ is defined it can be seen from (4.7) that ψ corresponds to a Lie dragging along χ by a distance Δ and therefore, in the limit $\Delta \rightarrow 0$ one gets the CSS condition.

Following [13], the coordinates used in (1.7) are transformed according to:

$$t \equiv e^\sigma T(\sigma, z) \quad (4.10)$$

$$r \equiv e^\sigma R(\sigma, z), \quad (4.11)$$

where $T(\sigma, z) = T(\sigma + \Delta, z)$ and $R(\sigma, z) = R(\sigma + \Delta, z)$ and z is a radial component in $x^a = (z, \theta, \varphi)$. Line element (1.7) in these new coordinates becomes

$$ds^2 = e^{2\sigma} \left\{ -\alpha^2 [(T + T_{,\sigma}) d\sigma + T_{,z} dz]^2 + a^2 [(R + R_{,\sigma}) d\sigma + R_{,z} dz]^2 + R^2 d\Omega^2 \right\}, \quad (4.12)$$

where, to satisfy (4.8), the metric functions must satisfy:

$$\alpha(t, r) = \alpha(e^{n\Delta} t, e^{n\Delta} r) \quad (4.13)$$

$$a(t, r) = a(e^{n\Delta} t, e^{n\Delta} r). \quad (4.14)$$

One final coordinate transformation, $t \rightarrow \bar{t}(t)$ such that $\bar{\alpha} = dt/d\bar{t} \alpha$, completes the construction of a DSS space-time.

The discussion here provides the basics for constructing a general DSS solution. There are many coordinates which satisfy the above conditions. For a more complete discussion of specific cases the reader is referred to Gundlach [17], [13].

Unlike the self-similarity property, the black hole mass scaling law (1.1) has analogies in other areas of physics. In statistical mechanics, for example, when the temperature of a gas is at its critical temperature, the law

$$|P - P_{cr}| \sim |v - v_{cr}|^\delta \quad (4.15)$$

holds where the left-hand-side is a difference in pressures and the right-hand-side is a difference in specific volumes. Similar mathematical properties are observed in studies of superconductivity and superfluidity in substances at low temperature. From experiment it is found that the value of the exponent for these laws depends on the particular gas or metal analogous to gravitational studies which indicate that γ is matter dependent (for example: compare results here with [6] and [18]).

Analysis on the scaling law can be done via perturbational techniques on the critical solution [19], [13]. In [19] a dominant linear perturbation mode is found numerically ($\gamma = 0.3558019$) for a perfect radiation fluid. In [13], a DSS space-time is subjected to a perturbation yielding a value of $\gamma = 0.374$. Both results are in agreement with the study done here. In the DSS case studied in [13] a periodic wiggle in the scaling law is found with a period in the quantity $\ln(p - p^*)$ of $\Delta/2\gamma \approx 4.61$, where $\Delta \equiv \ln \Delta_t$.

5. **Concluding Remarks**

I begin this section with a summary. A numerical scheme was employed which follows the collapse of a massless scalar field in a spherically symmetric space-time. The scheme does not use adaptive mesh refinement but instead utilizes null coordinates along with an adaptive quadrature technique on a number of different initial data surfaces. DSS in the field variable h was found when the system was evolved at criticality. Also, at barely subcritical the light cone structure near the origin becomes less steep at late times (u approaches u^* , the time corresponding to black hole formation). This behaviour is opposite to what one would expect when the conditions are this close to black hole formation.

At supercritical values of p the masses of black holes which form follow the power law $M = k(p - p^*)^\gamma$ where γ is independent of initial conditions within the class of matter studied here. Analogies between this power law behaviour and phase transitions from statistical mechanics have also been presented.

There are some factors which affect the applicability of such a system to the real universe. After all, a massless scalar field is a very simple matter model unlike the matter which undergoes gravitational collapse in the cosmos. This aside, there will rarely be initial conditions anywhere in the universe that will allow the formation of infinitesimal mass black holes. It should be stressed that theoretical studies such as this one are to be used to aide in the understanding

of phenomena which are too complex given the mathematical formulation of the problem and computing power of the present day. Other forms of matter in other symmetries also show some of the properties found here (for example: see [7]) indicating that the phenomena are neither a product of the choice of matter or the space-time symmetries.

The numerical method employed here has both advantages and disadvantages over other techniques. There is the advantage of simplicity that the null formulation provides over adaptive mesh methods (along with a considerable speed advantage) while the adaptive quadrature algorithm provides a simple and quick way for the user to increase resolution if needed (as in the study of the light cone structure near the origin). The disadvantages come from having to "fine-tune" initial conditions to ensure that the critical details are resolved throughout the evolution.

The code was developed in C on an Intel 486 processor. Once the program was working all runs (profiles a to d) were executed on a SUN SparcStation-10 for greater speed and accuracy.

6.

Appendices

6.1. Appendix A: Derivation of formulae

6.1.1. The Wave Equation from the Lagrangian Density:

The Lagrangian density for a massless scalar field in the presence of gravitation is:

$$\begin{aligned}\mathcal{L} &= \sqrt{-g} \frac{1}{2} (g^{\mu\nu} \phi_{,\mu} \phi_{,\nu}) \\ &= \sqrt{-g} \frac{1}{2} (\phi^{;\mu} \phi_{,\mu}).\end{aligned}\tag{6.1}$$

Lagrange's equations for continuous systems are:

$$\frac{\partial \mathcal{L}}{\partial x^\alpha} \left[\frac{\partial \mathcal{L}}{\partial (\phi_{,\alpha})} \right] - \frac{\partial \mathcal{L}}{\partial \phi} = 0,\tag{6.2}$$

Since ϕ is a scalar, the usual partial derivative can be replaced by the covariant derivative. Now,

$$\frac{\partial \mathcal{L}}{\partial \phi} = 0, \quad \frac{\partial \mathcal{L}}{\partial (\phi_{,\alpha})} = \sqrt{-g} \frac{1}{2} (\phi_{;\nu} g^{\mu\nu} \delta_\mu^\alpha + \phi_{;\mu} g^{\mu\nu} \delta_\nu^\alpha) = \sqrt{-g} \phi^{;\alpha}\tag{6.3}$$

therefore, Lagrange's equations become:

$$\begin{aligned}
\frac{\partial \mathcal{L}}{\partial x^\alpha} \left[\frac{\partial \mathcal{L}}{\partial (\phi_{;\alpha})} \right] &= (\sqrt{-g} \phi^{;\alpha})_{;\alpha} \\
&= \sqrt{-g} \phi^{;\alpha}{}_{;\alpha} = 0 \\
&\Rightarrow \phi^{;\alpha}{}_{;\alpha} = 0
\end{aligned} \tag{6.4}$$

6.1.2. The Stress Energy Tensor from the Lagrangian Density:

From field theory,

$$T_{\beta}^{\alpha} = \frac{1}{\sqrt{-g}} \left[\frac{\partial \mathcal{L}}{\partial (\phi_{;\alpha})} \phi_{;\beta} - \mathcal{L} \delta_{\beta}^{\alpha} \right]. \tag{6.5}$$

Using the Lagrangian density given above,

$$\begin{aligned}
\frac{\partial \mathcal{L}}{\partial (\phi_{;\alpha})} &= \sqrt{-g} \frac{1}{2} (\phi_{;\nu} g^{\mu\nu} \delta_{\mu}^{\alpha} + \phi_{;\mu} g^{\mu\nu} \delta_{\nu}^{\alpha}) \\
&= \sqrt{-g} \phi^{;\alpha},
\end{aligned} \tag{6.6}$$

and

$$\mathcal{L}\delta_{\beta}^{\alpha} = \sqrt{-g}\frac{1}{2}(\phi^{;\mu}\phi_{;\mu})\delta_{\beta}^{\alpha}. \quad (6.7)$$

Therefore (6.5) becomes:

$$T_{\beta}^{\alpha} = \frac{1}{\sqrt{-g}} \left[\sqrt{-g}\phi^{;\alpha}\phi_{;\beta} - \sqrt{-g}\frac{1}{2}(\phi^{;\mu}\phi_{;\mu})\delta_{\beta}^{\alpha} \right], \quad (6.8)$$

which, after lowering α and cancelling the denominator, becomes:

$$T_{\alpha\beta} = \phi_{;\alpha}\phi_{;\beta} - \frac{1}{2}(g_{\alpha\beta}\phi^{;\mu}\phi_{;\mu}). \quad (6.9)$$

6.1.3. The Wave Equation from the Conservation Law:

From (6.9) with partial derivatives replaced by covariant derivatives,

$$\begin{aligned} 0 &= T^{;\beta}{}_{\alpha\beta} = \phi^{;\beta}{}_{;\alpha}\phi_{;\beta} + \phi_{;\alpha}\phi^{;\beta}{}_{;\beta} - \frac{1}{2}g_{\alpha\beta}(\phi^{;\mu;\beta}\phi_{;\mu} + \phi^{;\mu}\phi^{;\beta}{}_{;\mu}) \\ &= \phi^{;\beta}{}_{;\alpha}\phi_{;\beta} + \phi_{;\alpha}\phi^{;\beta}{}_{;\beta} - \frac{1}{2}(\phi^{;\mu}{}_{;\alpha}\phi_{;\mu} + \phi^{;\mu}\phi_{;\mu;\alpha}) \\ &= \phi^{;\beta}{}_{;\alpha}\phi_{;\beta} + \phi_{;\alpha}\phi^{;\beta}{}_{;\beta} - \frac{1}{2}(\phi^{;\mu}{}_{;\alpha}\phi_{;\mu} + \phi_{;\kappa}\phi^{;\beta}{}_{;\alpha}g^{\kappa\mu}g_{\beta\mu}). \end{aligned} \quad (6.10)$$

Which, after re-labeling dummy indices,

$$\begin{aligned}
&= \phi_{;\alpha} \phi^{;\beta}{}_{;\beta} = 0 \\
&\Rightarrow \phi^{;\beta}{}_{;\beta} = 0.
\end{aligned} \tag{6.11}$$

6.1.4. The Evolution Law for \bar{h} :

For simplicity in notation, define the operator D such that

$$D \equiv \frac{\partial}{\partial u} - \frac{1}{2\bar{g}} \frac{\partial}{\partial r}. \tag{6.12}$$

The evolution law for the quantity $r\bar{h}$ is given by (from the definition of \bar{h} as a function of h):

$$\begin{aligned}
D(r\bar{h}) &= D\left(\int_0^r h dr'\right) \\
&= \frac{\partial}{\partial u} \left(\int_0^r h dr'\right) - \frac{1}{2\bar{g}} \frac{\partial}{\partial r} \left(\int_0^r h dr'\right) \\
&= \int_0^r \frac{\partial h}{\partial u} dr' - \frac{1}{2}\bar{g}h.
\end{aligned} \tag{6.13}$$

From the evolution law for h we get,

$$\frac{\partial h}{\partial u} = \frac{1}{2r} (g - \bar{g}) (h - \bar{h}) + \frac{1}{2} \bar{g} \frac{\partial h}{\partial r}, \quad (6.14)$$

and we can therefore write:

$$D(r\bar{h}) = \int_0^r \left[\frac{1}{2} \left(\frac{g - \bar{g}}{r'} \right) (h - \bar{h}) + \frac{1}{2} \bar{g} \frac{\partial h}{\partial r'} \right] dr' - \frac{1}{2} \bar{g} h. \quad (6.15)$$

Recall that $\frac{\partial \bar{I}}{\partial r} = \left(\frac{I - \bar{I}}{r} \right)$ and therefore, the above can be rewritten as

$$D(r\bar{h}) = \int_0^r \left[\frac{1}{2} \frac{\partial \bar{g}}{\partial r'} (h - \bar{h}) + \frac{1}{2} \bar{g} \frac{\partial h}{\partial r'} \right] dr' - \frac{1}{2} \bar{g} h. \quad (6.16)$$

Multiplying out the terms and integrating by parts yields,

$$\begin{aligned} D(r\bar{h}) &= \frac{1}{2} [h\bar{g}]_{r'=0}^{r'=r} - \frac{1}{2} \int_0^r \bar{g} \frac{\partial h}{\partial r'} dr' - \frac{1}{2} \int_0^r \frac{\partial \bar{g}}{\partial r'} \bar{h} dr' \\ &\quad + \frac{1}{2} \int_0^r \bar{g} \frac{\partial h}{\partial r'} dr' - \frac{1}{2} \bar{g} h \\ &= -\frac{1}{2} [h\bar{g}]_{r'=0} - \frac{1}{2} \int_0^r \frac{\partial \bar{g}}{\partial r'} \bar{h} dr'. \end{aligned} \quad (6.17)$$

Integrating the last term by parts and noting that $h(u, 0) = \bar{h}(u, 0)$ gives:

$$\begin{aligned}
D(r\bar{h}) &= -\frac{1}{2}\bar{g}\bar{h} + \frac{1}{2}\int_0^r \bar{g}\frac{\partial\bar{h}}{\partial r'}dr' \\
&= -\frac{1}{2}\bar{g}\bar{h} + \frac{1}{2}\int_0^r \bar{g}\left(\frac{h-\bar{h}}{r'}\right)dr'.
\end{aligned}
\tag{6.18}$$

Now, writing out the left-hand-side in long form as

$$D(r\bar{h}) = r\frac{\partial\bar{h}}{\partial u} - \frac{1}{2}\bar{g}\bar{h} - \frac{1}{2}r\bar{g}\frac{\partial\bar{h}}{\partial r} \tag{6.19}$$

and comparing with the last line in (6.18), we can conclude that the evolution law for \bar{h} is:

$$\frac{\partial\bar{h}}{\partial u} - \frac{1}{2}\bar{g}\frac{\partial\bar{h}}{\partial r} = \frac{1}{2r}\int_0^r \bar{g}\left(\frac{h-\bar{h}}{r'}\right)dr'. \tag{6.20}$$

6.1.5. Quantities Near the Origin:

h is expanded as

$$h \approx h_0 + h_1r + O(r^2). \tag{6.21}$$

Therefore, from the definition of \bar{h} ,

$$\begin{aligned}\bar{h} &= \frac{1}{r} \int_0^r (h_0 + h_1 r') dr' \\ &= h_0 + \frac{h_1 r}{2}.\end{aligned}\tag{6.22}$$

For g :

$$g = \exp \left[4\pi \int_0^r \frac{(h - \bar{h})^2}{r'} dr' \right].\tag{6.23}$$

Substituting (6.21) and (6.22) in (6.23):

$$\begin{aligned}g &= \exp \left[4\pi \int_0^r \frac{(h_1 r' - \frac{h_1 r'}{2})^2}{r'} dr' \right] \\ &= \exp \left[\pi \int_0^r (h_1^2 r') dr' \right] \\ &= \exp \left[\pi h_1^2 \frac{r^2}{2} \right].\end{aligned}\tag{6.24}$$

Expanding the last term in a Taylor series in r yields,

$$1 + \frac{\pi h_1^2 r^2}{2} + O(r^4).\tag{6.25}$$

From the definition of \bar{g} ,

$$\begin{aligned}\bar{g} &= \frac{1}{r} \int_0^r \left(1 + \frac{\pi h_1^2 r'^2}{2} \right) dr' \\ &= 1 + \frac{\pi}{6} h_1^2 r^2.\end{aligned}\tag{6.26}$$

6.1.6. Curvature Scalar Near the Origin:

With $G = c = 1$, the Ricci scalar for the massless scalar field is given by:

$$R = 8\pi (\phi_{,\alpha} \phi^{,\alpha}).\tag{6.27}$$

From [14],

$$(\phi_{,\alpha} \phi^{,\alpha}) = -2e^{-v-\lambda} \phi_{,u} \phi_{,r} + e^{-2\lambda} (\phi_{,r})^2.\tag{6.28}$$

Which becomes, after substituting g and \bar{g} (see main text):

$$\frac{-2}{g} \phi_{,u} \phi_{,r} + \frac{\bar{g}}{g} (\phi_{,r})^2.\tag{6.29}$$

Now, $\phi \equiv \bar{h}$ which, near the origin, is given by (6.22) while regularity at the origin requires $g = \bar{g} = 1$. Therefore, (6.27) becomes:

$$\begin{aligned} R &= 8\pi \left(\frac{h_1}{2}\right)^2 & (6.30) \\ &= 2\pi h_1^2. \end{aligned}$$

6.2. Appendix B: Computer Code

```
/* a C program that will evolve the gravitational collapse of */
/* h (=d/dr (r*hbar)) (where hbar is the scalar field) using an */
/* adaptive quadrature technique. */
/* The space-time is spherically symmetric. */

#include <stdlib.h>
#include <stdio.h>
#include <math.h>

#define PI 3.1415926535897932
#define euler 2.718281828459045235
#define TOLERANCE 0.000000002600
#define SIGMA 5E-1
#define rb -.01 /* centre of first bump */
#define rc 2 /* centre of second bump */

double adapt(double a, double b);
double simpsons(double a,double b,int N);
void assignrad(double rad);
void comphbar();
```

```
void compgs();

double AMPmax=2.8682500000000000E-1;

double AMPmin=2.8682100000000000E-1;

double AMP; /* the CRITICAL (!! ) parameter */

double r[500]; /* the radii */

double h[500]; /*differential of the scalar field */

double g[500];

double hscale[500];

double hbar[500];

double gbar[500];

double rrst[500];

double hrst[500];

double wgt[500];

double aint[500];

double rnew[500];

double hnew[500];

double dq;

double dv;

static int zeta;
```

```
double ktime;

double cmax,time,ktimeo;

double umax=5.6667615395;

double ntime=12000; /* number of evolution steps */

int nprint=1;

int iprint=50;

double xtime;

double h1;

double u;

double dsc;

double rsc;

double wt1, wt2;

int kr;

int krmin;

int inew;

int iscale;

double discale;

double rmax=4.0700;

double bondi;
```

```

double bhmass;

double schw;

int imin;

double tscale;

double curv;

double tmax;

/*-----*/

double adapt(double a, double b) /* checks accuracy of integration */
{
    double x=simpsons(a,b,10); /* the interval evaluated with 10 partitions */
    double y=simpsons(a,b,5); /* the interval evaluated with 5 partitions */
    if (fabs(x-y) > TOLERANCE)
        return adapt(a,(a+b)/2) + adapt((a+b)/2,b);
    else {
        double w=(b-a)/10; /* partition width for this specific interval */
        int i;
        for (i=0; i < 10; i++)
            {

```



```

        double MP =((a+i*w)+(a+i*w+w))/2; /* the ten radii for this in-
terval */

        assignrad(MP);

    }

    return x;

}

}

/* _____ */

```

```

double simpsons(double a,double b,int N) /*evaluates using Simpsons rule*/
{
    double s=0; /* the value of the integral */
    int i; /* which rectangle is being evaluated */
    double w=(b-a)/N; /* the width of the partitions */
    extern double AMP;
    for (i=0; i < N; i++)
    {
        double first=(a+i*w);
        double last=(a+i*w+w);
        double MP =(first+last)/2; /* the midpoint */

```

```

double c=3*AMP*pow(first,2)*(1/(-1 + pow(euler,(first - rb)/
SIGMA))+ 0.02*first/pow(euler,pow(first - rc,2)/
pow(SIGMA,2))) +AMP*pow(first,3)*(0.02/
pow(euler,pow(first - rc,2)/pow(SIGMA,2)) -
0.04*first*(first - rc)/(pow(euler,pow(first - rc,2)
/pow(SIGMA,2))*pow(SIGMA,2)) -pow(euler,(first - rb)
/SIGMA)/(pow(-1 + pow(euler,(first - rb)/SIGMA),2)*SIGMA));

double d=3*AMP*pow(MP,2)*(1/(-1 + pow(euler,(MP - rb)/
SIGMA))+0.02*MP/pow(euler,pow(MP - rc,2)/
pow(SIGMA,2))) +AMP*pow(MP,3)*(0.02/
pow(euler,pow(MP - rc,2)/pow(SIGMA,2)) -
0.04*MP*(MP - rc)/(pow(euler,pow(MP - rc,2)/
pow(SIGMA,2))*pow(SIGMA,2)) -pow(euler,(MP - rb)
/SIGMA)/(pow(-1 + pow(euler,(MP - rb)/SIGMA),2)*SIGMA));

double e=3*AMP*pow(last,2)*(1/(-1 + pow(euler,(last - rb)
/SIGMA))+0.02*last/pow(euler,pow(last - rc,2)/
pow(SIGMA,2))) +AMP*pow(last,3)*(0.02/
pow(euler,pow(last - rc,2)/pow(SIGMA,2)) -
0.04*last*(last - rc)/(pow(euler,pow(last - rc,2)

```

```

    /pow(SIGMA,2))*pow(SIGMA,2)) -pow(euler,(last - rb)/
    SIGMA))/(pow(-1 + pow(euler,(last - rb)/SIGMA),2)*SIGMA));

    s =s+((w/6)*((c)+4*(d)+(e)));

    }

return s;

}

/*-----*/

void assignrad(double rad) /* assigns initial radii to array */
{
    /* and initial h[i] to array */

    extern double AMP;

    extern double r[500];

    extern double h[500];

    extern int zeta;

    zeta++;

    r[zeta]=rad;

    h[zeta]=3*AMP*pow(r[zeta],2)*(1/(-1 + pow(euler,(r[zeta] - rb)
    /SIGMA)) +0.02*r[zeta]/pow(euler,pow(r[zeta] - rc,2)/
    pow(SIGMA,2)))+AMP*pow(r[zeta],3)*

```

```

(0.02/pow(euler,pow(r[zeta] - rc,2)/pow(SIGMA,2))
-0.04*r[zeta]*(r[zeta] - rc)/(pow(euler,pow(r[zeta] - rc,2)/
pow(SIGMA,2))*pow(SIGMA,2)) -pow(euler,(r[zeta] - rb)/SIGMA)/
(pow(-1 + pow(euler,(r[zeta] - rb)/SIGMA),2)*SIGMA));
}

/*-----*/

void main()
{
double chi;

double a;

int iv;

int k;

int i;

int irst;

int iodd;

int itime;

int irad;

int ii;

extern double AMPmax;

```

```
extern double AMPmin;
extern double AMP;
extern double dv;
extern double bhmass;
extern double bondi;
extern double schw;
extern int inew;
extern int iscale;
extern double discal;
extern int kr;
extern int krmin;
extern int imin;
extern int nprint;
extern int iprint;
extern double ntime;
extern double time;
extern double xtime;
extern double ktime;
extern double h[500];
```

```
extern double hscale[500];  
  
extern double r[500];  
  
extern double rrst[500];  
  
extern double hrst[500];  
  
extern double wgt[500];  
  
extern double rnew[500];  
  
extern double hnew[500];  
  
extern double u;  
  
extern double umax;  
  
extern double dsc;  
  
extern double rsc;  
  
extern double wt1,wt2;  
  
extern double dq;  
  
extern double tscale;  
  
int tuning=4;  
  
int ihalve;  
  
extern int zeta;  
  
FILE *pFileh=NULL;  
  
FILE *pFiler=NULL;
```

```

FILE *pFiles=NULL;

FILE *pFiled=NULL;

FILE *pFilet=NULL;

for (ihalve=1; ihalve<=100; ihalve++) /* The tuning cycle */
{
printf("running tuning cycle %i\n",ihalve);

if (tuning==95)
goto delete;

one:

AMP=(AMPmax+AMPmin)/2;

/* AMP=2.86823386684018E-1; Specific Amplitudes Defined Here */

cmax=0;

time=0;

ktimeo=0;

tscale=58;

zeta=0;

pFileh=fopen("sclrh","a");

pFiler=fopen("sclrr","a");

pFiles=fopen("hscale","a");

```

```

pFiled=fopen("data","a");
pFilet=fopen("time","a");
tuning=95;
imin=1;
chi=adapt(0,rmax); /* integrate from r=0 to rmax */
printf("\nThe value of integral using tolerance of %.20f is %.18f\n"
,TOLERANCE,chi);
printf("zeta=%i\n \n",zeta);
/* exit(0); */
/* ----- Time Evolution Loop ----- */
for (iv=1; iv<=ntime; iv++)
{
iprint++;
if (iprint==(nprint+50))
{
for (i=1; i<=zeta; i=i+5)
{
fprintf(pFileh, "%.20f ",h[i]);
fprintf(pFiler, "%.20f\n",r[i]);
}
}
}

```



```

    }

nprint=iprint;

fprintf(pFileh, "\n");

}

inew=imin;

for (k=imin; k<=zeta; k++)

{

if (r[k]>0)

    continue;

inew=k+1;

}

imin=inew;

if (time >=umax)

    goto three;

xxtime=tscale*log(1-(time/umax));

ktime=1-xxtime;

if (ktime <= ktimeo)

    goto three;

if (ktime > 1600)

```

```

    goto three;

ktimeo=ktime;

for (k=1; k<=zeta; k=k+6)
    {
        hscale[k]=0;
    }

u=umax-time;

dsc=0.7/zeta;

krmin=imin+1;

for (iscale=1; iscale<= zeta; iscale++)
    {
        discale=iscale;

        rsc=u*dsc*discale;

        for (kr=krmin; kr<= zeta; kr++)
            {
                if (r[kr]<rsc)
                    continue;

                krmin=kr;

                wt1=(r[kr]-rsc)/(r[kr]-r[kr-1]);
            }
    }

```

```
wt2=(rsc-r[kr-1])/(r[kr]-r[kr-1]);  
hscale[iscale]=wt1*h[kr-1]+wt2*h[kr];  
goto two;  
}
```

```
break;
```

```
two:
```

```
continue;  
}
```

```
for (i=1; i<=zeta; i=i+6)
```

```
{  
    fprintf(pFiles, "%.20f\n", hscale[i]);  
}
```

```
three:
```

```
if (imin<=zeta/2)
```

```
    goto four;
```

```
for (irst=1; irst <=zeta/2; irst++)
```

```
{  
    rrst[2*irst]=r[(zeta/2)+irst];  
    hrst[2*irst]=h[(zeta/2)+irst];  
}
```

```

    }
for (iodd=1; iodd<=((zeta/2)-1); iodd++)
    {
    rrst[2*iodd+1]=0.5*(rrst[2*iodd]+rrst[2*iodd+2]);
    hrst[2*iodd+1]=0.5*(hrst[2*iodd]+hrst[2*iodd+2]);
    }
h[1]=0;
r[1]=0;
for (i=2; i<=zeta; i++)
    {
    r[i]=rrst[i];
    h[i]=hrst[i];
    }
imin=2;
inew=imin;
for (k=imin; k<=zeta; k++)
    {
    if (r[k]>0)
        continue;

```

```

    inew=k+1;

    }

    imin=inew;

four:
    for (k=imin+1; k<=(zeta-1); k++)
        {
            wgt[k]=pow((r[k+1]-r[k]),2)/(6*(r[k]-r[k-1])*(r[k+1]-r[k-1]));
        }

    comphbar();

    compgs();

    schw=1-(gbar[zeta]/g[zeta]);

    bondi=0.5*schw*r[zeta];

    for (ii=imin+1; ii<=zeta; ii++)
        {
            if (fabs(h[ii]) <= 1.0)
                continue;

            goto five;
        }

/* — updating r and h using evolution equations — */

```

```

dv=10;
for (k=imin+2; k<=zeta; k++)
{
dq=0.5*(r[k]-r[k-1])/gbar[k];
if (dq > dv)
continue;
dv=dq;
}
time=time+dv;
fprintf(pFilet, "%.20f \n",time);
for (k=imin; k<=zeta; k++)
{
rnew[k]=r[k]-0.5*dv*gbar[k];
a=0.5*(g[k]-gbar[k])/r[k];
hnew[k]= h[k]*exp(a*dv)+hbar[k]*(1-exp(a*dv));
}
for (k=1; k<=zeta; k++)
{
r[k]=0;

```

```

    h[k]=0;
}
for (k=imin; k<=zeta; k++)
{
    r[k]=rnew[k];
    h[k]=hnew[k];
}
} /* end of time evolution loop*/

goto six;

five:

    bhmass=bondi;

    fprintf(pFiled, "\n\nAmplitude=: %.20f\nA Black Hole Forms With Mass:
%.20f\n“
    ,AMP,bhmass);

    fprintf(pFiled, “Amplitude: %.20f\nZeta:%i\nMaximum Curvature:
%.20f At Time: %.20f\n“,AMP,zeta,cmax,tmax);

    printf(“\n A Black Hole Forms With Mass: %.20f\n“,bhmass);

    if ((AMPmax-AMPmin)<2E-16)

        AMP=AMPmin;

```

```
AMPmax=AMP;
```

```
fclose(pFileh);
```

```
fclose(pFiler);
```

```
fclose(pFiles);
```

```
fclose(pFiled);
```

```
fclose(pFilet);
```

```
continue;
```

```
six:
```

```
fprintf(pFiled, "\nAmplitude: %.20f\nZeta:%i\nMaximum Curvature:
```

```
%.20f At Time: %.20f\n",AMP,zeta,cmax,tmax);
```

```
fprintf(pFiled, "rmax=%.20f\n",r[zeta]);
```

```
printf("rmax=r[%i]=%.20f\n",zeta,r[zeta]);
```

```
AMPmin=AMP;
```

```
fclose(pFileh);
```

```
fclose(pFiler);
```

```
fclose(pFiles);
```

```
fclose(pFiled);
```

```
fclose(pFilet);
```

```
if ((AMPmax-AMPmin)<2E-16)
```



```

    exit(0);

} /* end tuning loop */

exit(0);

delete:

remove("sclrr");

remove("sclrh");

remove("hscale");

remove("time");

goto one;

}

/*-----*/

void comphbar() /* computes evolved values of the scalar field */
{
    extern double h[500];

    extern double r[500];

    extern double hbar[500];

    extern double wgt[500];

    extern int nprint;

```

```
extern int iprint;

extern int imin;

int k;

int navg;

double havg;

double ravg;

double hravg;

double rsqavg;

extern double h1;

double hsum;

double crcl,crc2;

extern double curv;

extern double tmax;

extern int zeta;

FILE *pFilec=NULL;

pFilec=fopen("curvat ","a");

navg=4;

havg=0;

ravg=0;
```

```

hravg=0;

rsqavg=0;

for (k=imin+1; k<=imin+navg; k++)
    {
    havg=havg+h[k];

    ravg=ravg+r[k];

    hravg=hravg+(h[k]*r[k]);

    rsqavg=rsqavg+pow(r[k],2);

    }

havg=havg/navg;

ravg=ravg/navg;

hravg=hravg/navg;

rsqavg=rsqavg/navg;

h1=(hravg-havg*ravg)/(rsqavg-pow(ravg,2));

curv=2*PI*pow(h1,2);

fprintf(pFilec, "%.20f,\n",curv);

fclose(pFilec);

if (curv > cmax)

    tmax=time;

```

```

if (curv > cmax)

    cmax=curv;

hbar[imin]=h[imin]-0.5*h1*r[imin];

hbar[imin+1]=h[imin+1]-0.5*h1*r[imin+1];

hbar[imin+2]=h[imin+2]-0.5*h1*r[imin+2];

hsum=hbar[imin+2]*r[imin+2];

for (k=imin+3; k<=zeta; k++)

    {

        crc1=(r[k]-r[k-1])*(h[k-1]-h[k-2]);

        crc2=(r[k-1]-r[k-2])*(h[k-1]-h[k]);

        hsum=hsum+0.5*(h[k]+h[k-1])*(r[k]-r[k-1])+wgt[k-1]*(crc1+crc2);

        hbar[k]=hsum/r[k];

/* fprintf(pFileb, "%.20f\n", hbar[k]); */

    }

/* fclose(pFileb); */

}

/*-----*/

void compgs()

{

```

```

extern double g[500];

extern double gbar[500];

extern double aint[500];

extern double wgt[500];

extern int imin;

double asum;

extern double h1;

int k;

double crc1,crc2;

double gsum;

extern int zeta;

g[imin]=1+0.5*PI*(h1*pow(r[imin],2));

g[imin+1]=1+0.5*PI*(h1*pow(r[imin+1],2));

g[imin+2]=1+0.5*PI*(h1*pow(r[imin+2],2));

asum=0.5*PI*pow(h1*r[imin+2],2);

for (k=imin+1; k<=zeta; k++)

{

    aint[k]=(4.0*PI*pow((h[k]-hbar[k]),2))/r[k];

}

```

```

for (k=imin+3; k<=zeta; k++)
{
    crc1=(r[k]-r[k-1])*(aint[k-1]-aint[k-2]);
    crc2=(r[k-1]-r[k-2])*(aint[k-1]-aint[k]);
    asum=asum+0.5*(aint[k]+aint[k-1])*(r[k]-r[k-1])+wgt[k-1]*
    (crc1+crc2);
    g[k]=exp(asum);
}
gbar[imin]=1-(PI/6)*pow((h1*r[imin]),2);
gbar[imin+1]=1-(PI/6)*pow((h1*r[imin+1]),2);
gbar[imin+2]=1-(PI/6)*pow((h1*r[imin+2]),2);
gsum=gbar[imin+2]*r[imin+2];
for (k=imin+3; k<=zeta; k++)
{
    crc1=(r[k]-r[k-1])*(g[k-1]-g[k-2]);
    crc2=(r[k-1]-r[k-2])*(g[k-1]-g[k]);
    gsum=gsum+0.5*(g[k]+g[k-1])*(r[k]-r[k-1])+wgt[k-1]*
    (crc1+crc2);
    gbar[k]=gsum/r[k];
}

```

}
}

References

- [1] Matthew W. Choptuik. Universality and scaling in gravitational collapse of a massless scalar field. *Phys. Rev. Lett.*, 70(1):9–12, 1993.
- [2] M.J. Berger and J. Olinger. Adaptive mesh refinement for hyperbolic partial differential equations. *J. Comput. Phys.*, 53:484–512, 1984.
- [3] David Garfinkle. Choptuik scaling in null coordinates. *Phys. Rev. D*, 51:5558–5561, 1995.
- [4] Rufus S. Hamade and John M. Stewart. The spherically symmetric collapse of a massless scalar field. *Class. Quantum Gravity*, 13:497–512, 1996.
- [5] Eric W. Hirschmann and Douglas M. Eardley. Universal scaling and echoing in the gravitational collapse of a complex scalar field. *Phys. Rev. D*, 51:4198–4207, 1995.
- [6] Rufus Hamade, James H. Horne, and John M. Stewart. Continuous self-similarity and s-duality. gr-qc 9511024.
- [7] A.M. Abrahams and C.R. Evans. *Phys. Rev. Lett.*, 70:2980, 1993.

- [8] Shahar Hod and Tsvi Piran. Fine structure of choptuik's mass-scaling relation. gr-qc 9606087.
- [9] Shahar Hod and Tsvi Piran. Critical behaviour and universality in gravitational collapse of a charged scalar field. gr-qc 9606093.
- [10] H.P. DeOliveira. Self-similar collapse in brans-dicke theory and critical behaviour. gr-qc 9605008.
- [11] L.Liebling and Matthew W. Choptuik. Black hole criticality in brans-dicke model. gr-qc 9606057.
- [12] Richard H. Price and Jorge Pullin. Analytic approximations to the spacetime of a critical gravitational collapse. gr-qc 9601009.
- [13] Carsten Gundlach. Understanding critical collapse of a scalar field. unpublished as of April 1996.
- [14] Demetrios Christodoulou. The problem of a self-gravitating scalar field. *Commun. Math. Phys.*, 105:337–361, 1986.
- [15] Nick Kaiser. private communication to M.W. Choptuik.
- [16] P. Brady. Self-similar scalar field collapse: naked singularities and critical behaviour. *Phys. Rev. D*, 51:4168, 1995.

- [17] Carsten Gundlach. The choptuik spacetime as an eigenvalue problem. *Phys. Rev. Lett.*, 75:3214, 1995.
- [18] D. Maison. Non-universality of critical behaviour in spherically symmetric gravitational collapse. gr-qc 9504008.
- [19] T. Koike, T. Hara, and S. Adachi. Critical behaviour in gravitational collapse of radiation fluid—a renormalization group analysis. *Phys. Rev. Lett.*, 74:5170, 1995.

Vita Auctoris

NAME: Andrew DeBenedictis
PLACE OF BIRTH: Moncton, New Brunswick
YEAR OF BIRTH: 1971
EDUCATION: University of Victoria, Victoria, B.C.

1989-1990 (Chemistry)

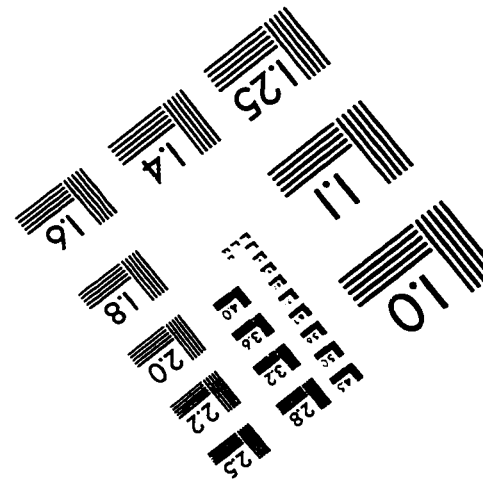
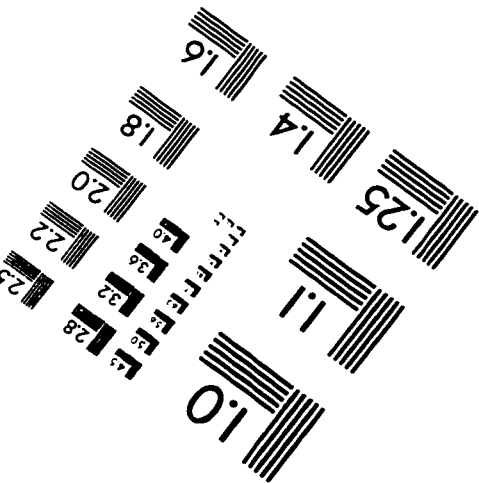
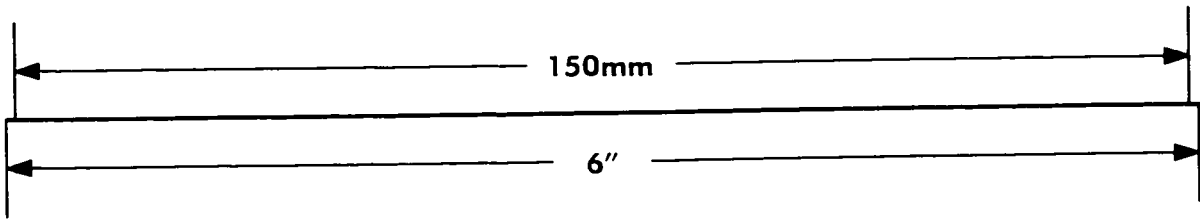
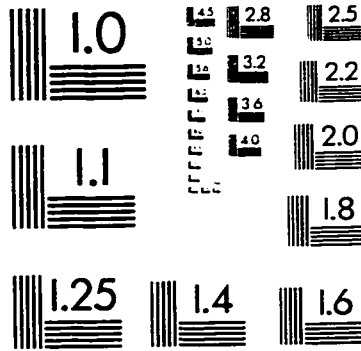
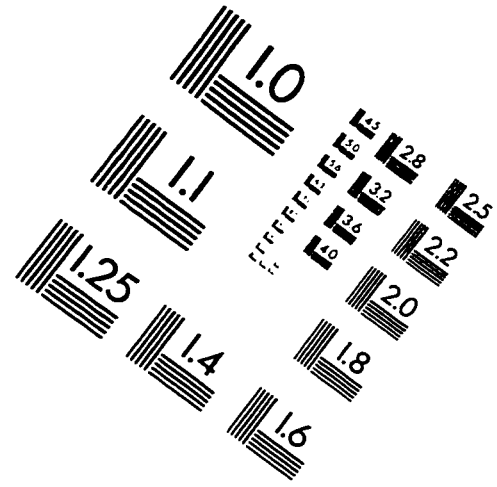
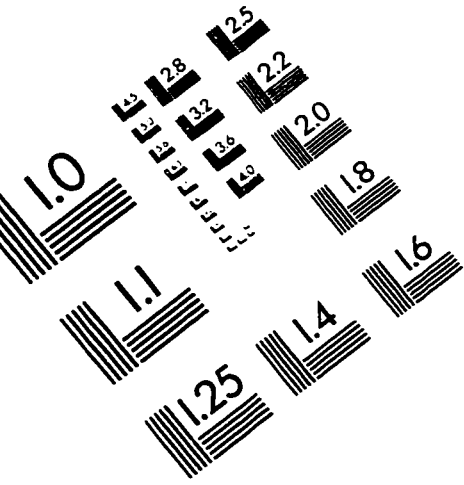
University of British Columbia, Vancouver, B.C.

1990-1995 B.Sc. (Honours Physics/Astronomy)

University of Windsor, Windsor, Ont.

1995-1996 M.Sc. (Physics)

IMAGE EVALUATION TEST TARGET (QA-3)



APPLIED IMAGE, Inc
1653 East Main Street
Rochester, NY 14609 USA
Phone: 716/482-0300
Fax: 716/288-5989

© 1993, Applied Image, Inc., All Rights Reserved